5G PPP

European Commission | Horizon 2020 European Union funding for Research & Innovation

5G-XHaul

Dynamically Reconfigurable Optical-Wireless Backhaul/Fronthaul with Cognitive Control Plane for Small Cells and Cloud-RANs

D4.13 Synchronization and localization for cooperative communications

This project has received funding from the European Union's Framework Programme Horizon 2020 for research, technological development and demonstration

Advanced 5G Network Infrastructure for the Future Internet

Project Start Date: July 1st, 2015 Duration: 36 months

H2020-ICT-2014-2 671551 July 1st, 2016 – Version 1.0

Project co-funded by the European Commission

Under the H2020 programme

Dissemination Level: Public

Grant Agreement Number:	671551
Project Name:	Dynamically Reconfigurable Optical-Wireless Back-haul/Fronthaul with Cognitive Control Plane for Small Cells and Cloud-RANs
Project Acronym:	5G-XHaul
Document Number:	D4.13
Document Title:	Synchronisation and Localisation for Cooperative Communications
Version:	1.0
Delivery Date:	March 31st, 2017 (April 4th, 2017)
Responsible:	**IHP**
Editor(s):	Vladica Sark (**IHP**), Jesús Gutiérrez (**IHP**)
Authors:	Vladica Sark (**IHP**), Jesús Gutiérrez (**IHP**), Eckhard Grass (**IHP**), Peter Legg (**BWT**), Stuart Ryan (**BWT**), Eduard García (**I2CAT-UPC**), Nikola Vucic (**HWDU**)
Keywords:	Synchronisation, Ranging, Positioning, Localisation, 1588, GPS, GNSS, Time-of-Flight, Time of Arrival
Status:	Final
Dissemination Level	Public
Project URL:	http://www.5g-xhaul-project.eu/

Table of Contents

List of Figures

List of Tables

Executive Summary

The 5G-XHaul project proposes a flexible transport infrastructure built on a converged optical and wireless network solution supported by a flexible and scalable control plane. This infrastructure will be able to jointly support backhaul (BH) and fronthaul (FH) functionalities required to cope with the future challenges imposed by fifth generation (5G) Radio Access Networks (RANs).

As described in the 5G-XHaul deliverable D2.2, the project considers multi-hop wireless transport topologies to convey the aggregated traffic within the network. The wireless connectivity scenarios proposed in this deliverable leverage the wireless technologies developed in the project, namely millimetre-wave (mmWave) and Sub-6. These technologies play a key role and provide the network with enough flexibility to cater the largely varying traffic loads expected for 5G.

Transport networks in 5G must experience a big leap in performance to underpin tighter transport performance requirements in relation to frequency synchronisation, phase synchronisation and latency performance. This will be partially possible by leveraging current available solutions, such as IEEE 1588, SyncE, etc. It is well known that the concepts of synchronisation and ranging/localisation technically are going hand in hand with each other, and synchronisation is a main issue in localisation applications. In this deliverable we will present the two concepts separately, keeping in mind the existing tight relation between them. One of the upsides for considering both concepts together is that both can benefit from the other, e.g. methods for localisation can significantly reduce the synchronisation requirements.

This deliverable first presents the synchronisation requirements for small cells, the different challenges as well as solutions currently available. The 5G-XHaul transport network will contain synchronisation functions that are required to support some of the concepts tackled in previous deliverables, e.g. the support of multiple functional splits.

On other hand, the 5G concept encompasses technologies which might benefit from cooperative positioning. 5G will definitely benefit from the research on positioning from both infrastructure and mobile users sides. 5G-XHaul will bring together concepts such as ranging and localisation with synchronisation, to identify and build up from their synergies, and to develop solutions in these areas concurrently with the development of wireless network technologies. The deliverable presents the state of the art in terms of wireless positioning methods, as well as the developed solutions to be used and integrated in the 5G-XHaul transport network.

From our perspective, this deliverable is better understood when bringing the two concepts together. As a matter of fact, the research on algorithms for both concepts will continue and the outcomes of their integration within the 5G-XHaul solution will be put forward in WP3 and WP5-related deliverables.

1 Introduction

5G mobile networks are expected to offer considerable enhancements such as significantly higher peak data rates, much improved area capacity, Internet of Things (IoT) support, ensuring low end-to-end latency, etc. To achieve these improvements, traditional Radio Access Networks (RANs) will evolve to alternative solutions, such as C-RAN, requiring increased transport bandwidth, and having strict latency and synchronisation constraints [1].

Network synchronisation is traditionally important to guarantee good performance in transport and mobile network operations, e.g. for user handovers in RANs, where frequency synchronisation plays an important role. The requirement for precise time synchronisation between different nodes is one of the challenges faced by today's wireless networks. The provision of accurate phase/time synchronisation has become of key importance, e.g. enabling the alignment of radio frames for a better use of radio resources.

Nowadays, positioning/localisation systems get synchronised with each other using hardware such as GPS receivers or atomic clocks, which are often expensive. In cases where this hardware is not available, synchronisation methods rely on message exchange protocols, which impose challenging synchronisation requirements. If fine synchronisation is not performed, these errors can affect the time measurements and, consequently, the location accuracy.

5G-XHaul, as outlined in deliverable D2.2, proposes a wireless architecture encompassing different transport scenarios, some of them requiring interaction not only between different nodes using the same technology but also between nodes using different technologies (see Figure 1). All these envisioned scenarios impose a set of requirements to this wireless architecture. The coexistence of these different wireless technologies, and the well-known diverse set of requirements expected at the architectural level in terms of data rate and latency (c.f. deliverables D2.1 [2], D2.2 [3]), clearly necessitate strict synchronisation methods.

As an example, key disadvantages of Cloud-RAN (C-RAN) are the increased transport bandwidth requirements as well as the strict latency and synchronisation constraints [1]. This means that the remote units (RUs) need to be connected to the compute resources responsible for baseband (BB) processing with very stringent delay and synchronisation requirements. Depending on the type of traffic and the underlying application, 5G-XHaul proposes to introduce different transport classes, with the aim to relax the stringent requirements in terms of transport capacity, delay and synchronisation.

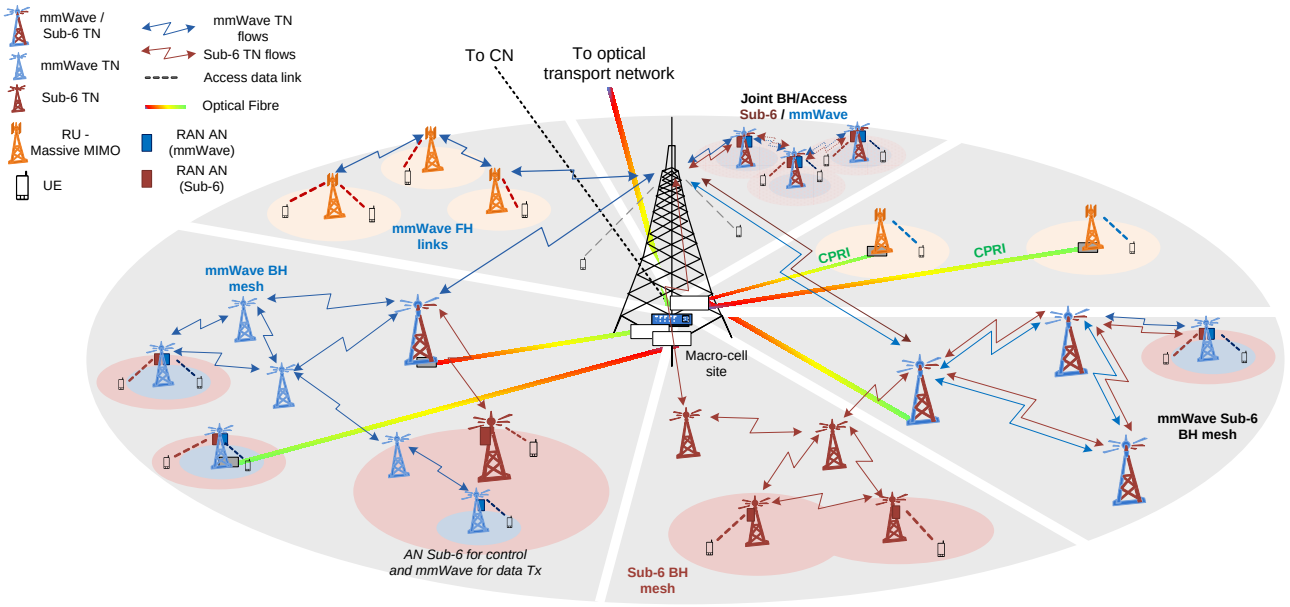

Figure 1: 5G-XHaul wireless connectivity scenarios. TN stands for Transport Node, representing a device with transport functions; and AN stands for Access Node, representing a device with RAN functions.

The expected network densification in 5G will play a key role for identifying the position of new small cells introduced in the network, as well as for the location of the user equipments (UEs). Very dense RANs, as envisioned in 5G, require a much closer interaction between the ANs and the mobile users [4] [5]. This, in principle, favours localisation, since the probability of having line-of-sight (LoS) scenarios increases. In addition, localisation can benefit from directionality in millimetre wave (mmWave) RF frequencies. Strong multipath propagation, LoS signal blockage, and unfavourable geometric satellite constellations, result in highly degraded positioning accuracies. MmWave technology, with its high signal bandwidth, supports achieving ranging precisions down to 1 cm. The Sub-6 technology will be able to provide precisions down to 1 metre.

The new RAN design allows introducing a new kind of performance indicator, which is UE positioning [6]. Location-based services (LBSs) are more and more used with the development of wireless communication and mobile Internet technology [7]. A positioning accuracy in the order of sub-meter is critical for a plethora of LBSs, as input for data analytics, to improve public safety in emergency scenarios, to introduce services like collision avoidance in autonomous vehicles, and to create new customised experiences and services for the end user.

It is expected that, since the research and implementations for 5G are still in an early stage, the wireless research community will consider positioning as an integral part of wireless technology development. The wide bandwidths and diverse carrier frequencies expected for 5G support the advent of highly accurate integrated positioning methods, e.g. based on Time of Arrival (ToA) and/or Direction of Arrival (DoA) estimates, which will benefit from strict synchronisation methods. All in all, 5G is in a good position to outperform and complement current positioning techniques such as global navigation satellite systems (GNSSs), with an accuracy of approx. 5 metres [8], LTE observed time difference of arrival (OTDoA), with approx. 7 metres precision [9], or WLAN fingerprinting (3 – 4 metres precision [10]).

This deliverable proposes synchronisation methods and techniques to be adopted in the 5G-XHaul wireless data plane. Moreover, it presents techniques to obtain the position of the nodes of the network aiming at low power consumption and complexity, with a negligible impact on the data rate.

Organisation of the document

The deliverable is structured in five main sections. Following the introduction section, Section 2 reviews the state-of-the-art in both synchronisation and localisation techniques, emphasizing earlier publications and studies related to cooperative wireless networks. Section 3 reviews the synchronisation requirements for 5G, delving into the different solutions currently available, as well as into the challenges with the most significant impact on transport networks. In Section 4, the ranging and localisation algorithms used in 5G-XHaul are presented, focusing first on the required parameters and needs, and hen presenting the algorithm development and implementation/integration in the wireless nodes. Section 5 focuses on the interoperability of the different 5G-XHaul nodes, explaining how the nodes interconnect and benefit from synchronisation and localisation. Finally, Section 6 provides a summary of the findings and the main conclusions of the deliverable are outlined.

2 State-of-the-Art in synchronisation and localisation

In 5G-XHaul we consider synchronisation as the distribution of common frequency and/or time references to the nodes present in a network to align their frequency and time scales, respectively. Both timing and synchronisation requirements quickly follow the evolution of both mobile and transport networks towards the definition of 5G. Assuming that the issue of frequency synchronisation and its distribution over the network has been covered with standards like 1588 and SyncE, still the current 4G Long Term Evolution (LTE) standards impose more stringent synchronisation requirements.

Timing and synchronisation bring normally the terms accuracy and precision to play, both achieved from a precise and accurate clock reference. A proper pair-wise time synchronisation between nodes in a wireless network can be achieved with the expected bandwidths considered in 5G. This fact also benefits localisation approaches, either based on ranging, connectivity, or angular information.

In the last couple of decades, Global Navigation Satellite Systems (GNSS) have become a very important part of our everyday life. Nevertheless, the offered localisation services are not available indoors and their performance is significantly affected in urban areas. Therefore, in the recent years, a large number of wireless localisation systems are being actively investigated and developed. As an example, current communication standards, e.g. LTE, provide already diverse positioning methods to complement GNSS-based localisation for mobile terminals.

This section presents the state of the art of both synchronisation and localisation technologies to be leveraged in the project.

2.1 Synchronisation methods

This section describes existing synchronisation technologies, explaining how they may be used to provide frequency and phase synchronisation.

2.1.1 GNSS (Global Navigation Satellite System)

As of December 2016, there are three operational GNSS systems: GPS, GLONASS (Russian) and Galileo (EU). GNSS satellites employ atomic clocks and this allows a GPS receiver itself to support atomic clock accuracy (with phase synchronisation of 50-100 ns, and frequency synchronisation of the order of 5 ppb). Clock delivery to other network nodes that do not possess GNSS (for example, they could be indoor small cells) can be achieved using SyncE or IEEE 1588 as described below. The GNSS equipped node can act as a grand master clock.

2.1.2 Methods for packet switched networks

The ITU [15][1][16][17] has identified two possible solutions for distributing precise frequency synchronisation across a packet switched network:

- Synchronous Ethernet (SyncE), uses a physical clock distribution to provide frequency synchronisation, but not phase synchronisation.
- IEEE 1588 defines a Precision Time Protocol (PTP) which provides both frequency and phase synchronisation.

2.1.2.1 SyncE

Synchronous Ethernet is a physical layer-based timing method that can provide frequency synchronisation of network nodes supporting Ethernet [15][11][21], i.e. a packet-based network. Synchronisation is achieved in a similar way to that used in SONET/SDH networks. Free-running clocks for the Ethernet PHY transmitters are swopped for phased-locked loops (PLLs). A high accuracy clock (known as stratum 1) is distributed by every node on a path recovering and re-transmitting the frequency synchronisation. The requirements on the PLLs are detailed in [11]. There are two options for SyncE, “EEC-Option 1” and “EEC-Option 2”, compatible with systems of the 2048 kb/s and 1544 kb/s hierarchies, respectively. In both cases the frequency accuracy should not be greater than 4.6 ppm.

An example of a chain of nodes synchronised to a primary reference clock is shown in Figure 2.

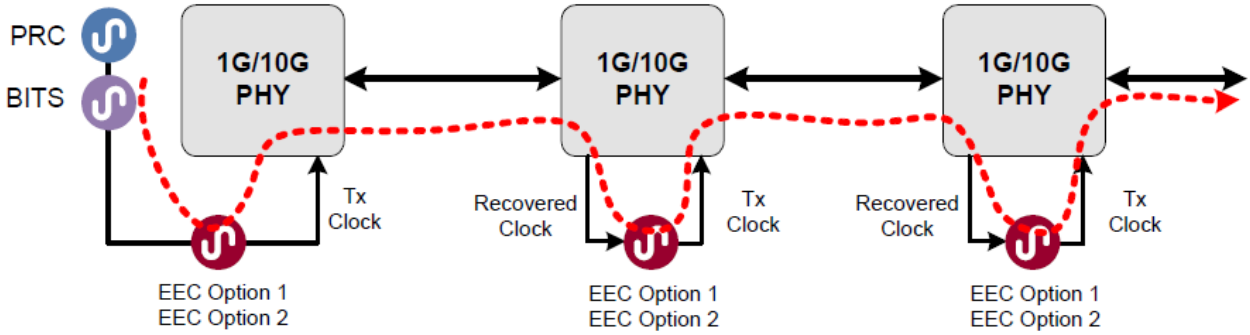

Figure 2: An example of clock recovery using SyncE, from [28], Primary Reference Clock (PRC), building integrated timing supply (BITS).

2.1.2.2 IEEE 1588

IEEE 1588 is a packet based timing method that relies on inserting time stamp packets amongst the user plane traffic. Time stamps may be inserted at the node where a master clock is located, and then extracted at nodes where a slave clock is placed. Unlike SyncE, 1588 is able to provide frequency and phase synchronisation. Additionally, intermediate nodes between the master and slave clocks need not be synchronous. Phase synchronisation exploits timing packets that are sent from the slave to the master to measure the round-trip time (RTT) – this value is halved to give the master to slave delay, although this is only precise if the exchange is symmetric. The accuracy of IEEE 1588 is limited by the packet delay jitter across the network and the asymmetry of the network.

An enhanced version of IEEE 1588, IEEE 1588v2 (aka IEEE 1588-2008), was introduced in 2008 to reduce the impact of packet delay variations. Time stamps are adjusted according to the estimated delay incurred by the timing packet through the node – this is called transparent clocking. With transparent clocking the accuracy improvements relies upon all nodes between master and slave supporting IEEE 1588v2.

The following clocks are used with IEEE 1588v2:

- Ordinary clock: has a single PTP port, it may be a master or synchronised to another clock as a slave.
- Boundary clock (BCL): has multiple PTP ports, may be a master or slave (if a slave it has a single slave port and transfers timing from that port to the master ports)
- Transparent clock (TCL): a device that measures the time for a PTP event message to transit the device (i.e. residence time), and provides this information to clocks receiving the PTP event message. PTP event messages are described in outline below. TCLs are not part of the master-slave hierarchy and do not synchronise with the master.

Transparent clocks can be peer-to-peer TCLs or end-to-end TCLs. The former additionally correct for propagation delay of the link connected to the port receiving the PTP event message. They also differ in the mechanisms employed to measure delay between master and slave clocks: using “peer delay” and “delay request-response” mechanisms, respectively. Example configurations are shown in Figure 3. Nodes ***A*** and ***C*** are ordinary clocks, whilst ***B*** is a BCL.

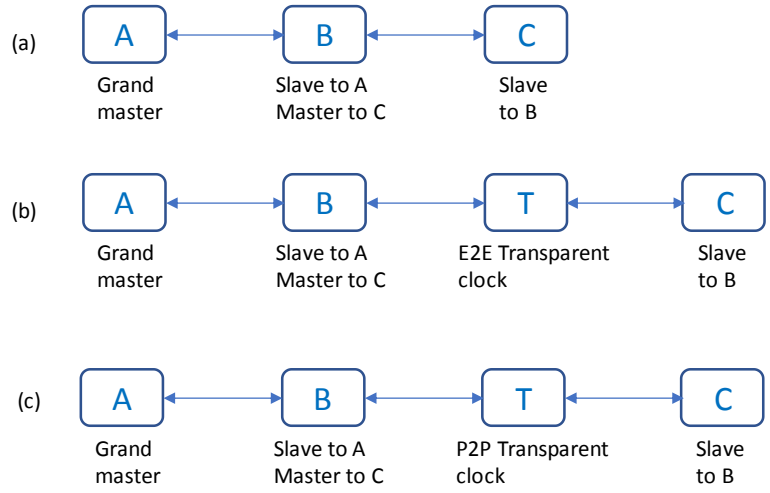

Figure 3: Example clock configurations for IEEE 1588v2.

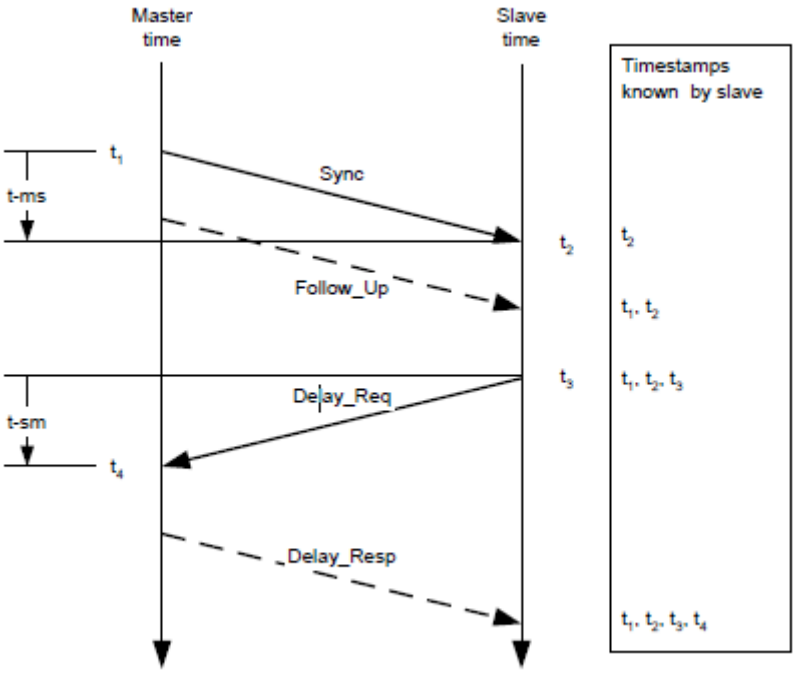

Figure 4: Exchange of PTP event messages as part of the delay request-response mechanism [17].

The delay request-response mechanism is shown below. The event message *Sync* is sent from master to slave. If the egress time stamp, t_1, can be included with sufficient accuracy, then its value is included in the *Sync* message, otherwise t_1 is carried in a separate Follow-up general message. The slave then sends a *Delay_Req* event message, to which the master replies with a general message, *Delay_Resp*, carrying t_4. Given the time stamps, the slave can calculate the offset between its clock and that of the master. If the link is not symmetric this offset is in error by the difference between the actual master-to-slave and mean propagation times.

Specific PTP profiles have been created to address telecom applications [18] [19], although some question whether it can achieve sub-microsecond phase synchronisation which is needed between antenna ports for transmit diversity and MIMO [20] [22] [23]. Profile G.8275.1 is for green-field deployments of IEEE 1588v2 such that BCs are located at every node except for grand masters and slaves. In G8275.2 IEEE 1588v2 exploits advanced BCs (these are BCLs with additional sync inputs like SyncE), and edge grand master clocks (these have GNSS input and are designed specifically for edge deployment). The clocks are deployed to limit the errors from path asymmetry.

2.1.3 Comparison of methods

The salient performance features of the methods discussed above are captured in Table 1.

Table 1: Comparison of synchronisation techniques.

	Frequency accuracy	Phase/time accuracy
GNSS	5 ppb	50-100 ns
SyncE	Can achieve that of the primary reference clock (PRC traceability), so similar to GNSS	Not supported
IEEE 1588v2	Much lower frequency accuracy than SyncE. Performance is dependent on the network's packet delay variation.	~1 us

2.2 Ranging and Localisation methods

The 5G concept and the envisioned wireless networks and technologies to be used in 5G are expected to benefit the development of high precision localisation methods. First, as a result of the high density of ANs, UEs in such networks are likely to have a LoS path towards multiple ANs for most of the time, even in demanding propagation environments. Such LoS conditions alone are already a very desirable property in positioning systems. Second, higher signal bandwidths allow better resolution of the wireless channel in time, which involves a more accurate estimation of the multipath components [41][42]. Finally, the use of directional antennas for wireless communications, i.e. antennas with narrower antenna beam width, is also an effective way of mitigating the effects of multipath propagation [43][44].

The task of developing a global high-precision positioning system is not trivial. When coverage of a large area is required, usually a high precision cannot be achieved. On the other hand, systems that have higher precision, usually do not have wide area coverage. For example, the GPS system has almost global coverage, but the precision is around 10 metres. In 5G, network-based positioning in three-dimensional space should be supported, with accuracy from 10 metres to <1 metre at 80% of occasions, and better than 1 metre for indoor deployments [24]. The positioning accuracy of 5G networks is expected to be in the order of one metre or even below [25] [24] [27].

Another important objective is to keep both cost and complexity as low as possible. The research within the 5G-XHaul project keeps this in mind when developing the algorithms and their subsequent implementation. The GPS, for example, has an atomic clock in every satellite, which is usually not suitable for implementation in small and portable devices, apart from increasing considerably their cost.

This section presents the most common localisation methods, and how these are supported by ranging algorithms, which are also briefly overviewed.

2.2.1 Localisation/Positioning methods

Localisation involves the estimation of a location (position) of an object in a given coordinate system. There exist different methods to perform localisation, as shown in Figure 5.

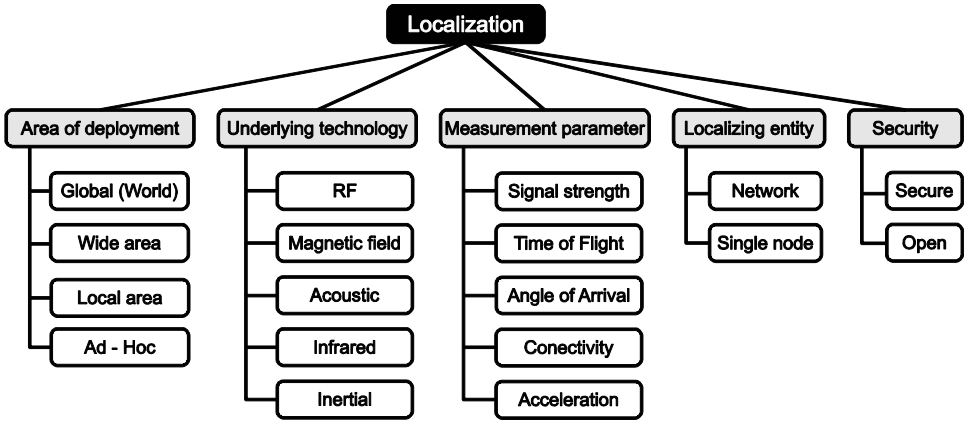

Figure 5: Classification of the localisation methods according to different criteria [46].

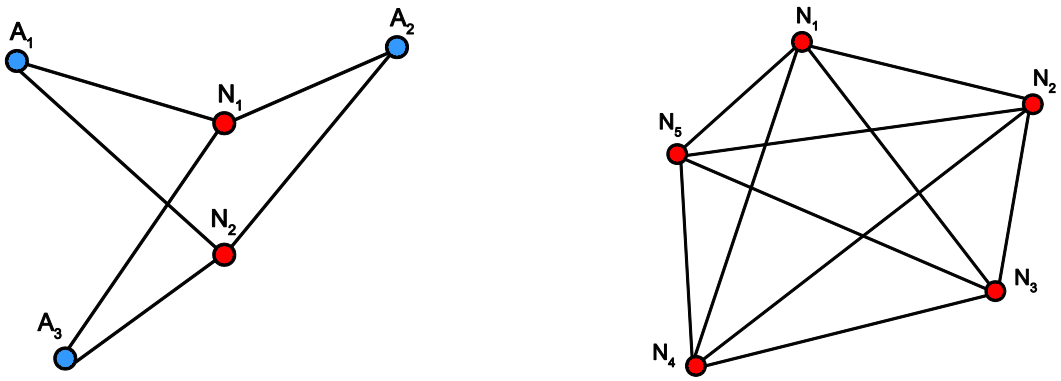

Figure 6: Classification of localisation approaches, a) Infrastructure-based localisation, b) Cooperative localisation.

In this deliverable we focus on RF localisation methods, i.e. localisation is performed using RF signals. These methods can be classified according to different criteria. Depending on the **devices used**, they can be classified as device-free localisation (DFL) and non-device-free localisation (NDFL). The DFL methods are used to estimate the position of an object (or human body) which does not have RF transmission capability. On the other hand, the NDFL methods are used to estimate the position of a device (or object) which is capable of RF transmission. In 5G-XHaul only the NDFL is of interest. Depending on the **deployed infrastructure**, localisation methods are classified as infrastructure-based localisation and infrastructure-free, as shown in Figure 6.

2.2.1.1 Infrastructure-based localisation

In infrastructure-based localisation (Figure 6a), wireless nodes with known position are used as reference nodes, and are commonly referred to as anchors or anchor nodes (A_1, A_2, …, A_N). The position of the other nodes (N_1, N_2, …, N_M) is estimated with respect to these known positions.

Trilateration

The commonly preferred localisation method is trilateration, mainly due to its simplicity. The basic trilateration method is shown in Figure 7a. It is based on range measurements from the unknown location to the anchor points with known coordinates. The distances (range) can be estimated by measuring different RF parameters, such as received power or radio signal propagation time, i.e. Time-of-Flight (ToF). Trilateration is also commonly used for position estimation in cooperative localisation scenarios. The positions of the nodes are estimated using the distances between the nodes.

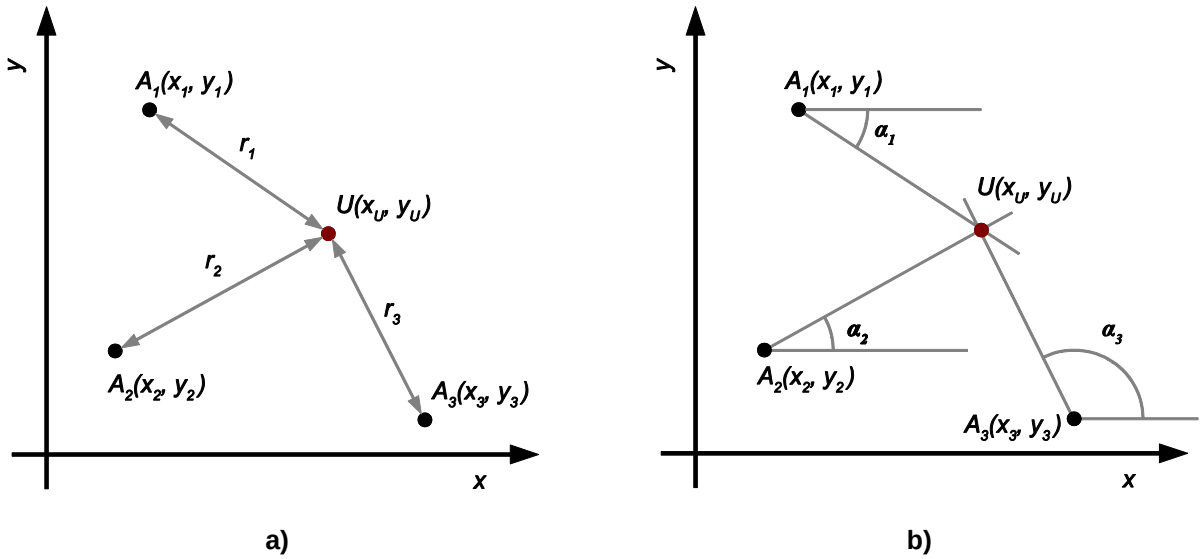

Figure 7: Trilateration and triangulation methods for location estimation: a) trilateration, b) triangulation.

Several different methods for estimating the coordinates of a node from distance measurements are available. Some good descriptions of these methods are given in [30], [31] and [33].

Triangulation

The triangulation method for location estimation is conceptually similar to the trilateration method. A simple illustration of the triangulation method is shown in Figure 7b. The unknown location is estimated by measuring the angles between the anchor points and the point with unknown location. The main complexity of triangulation comes from the need for antenna arrays at the wireless nodes to estimate the required angles. In addition, most of the radios with multiple antennas (or antenna arrays), do not usually have sufficient angle resolution, which is needed for precise localisation.

Combined angle of arrival (AoA) and time-of-flight (ToF) approach

In 5G, the ANs are expected to be equipped with smart antenna solutions, e.g. antenna arrays supporting multiple-input multiple-output (MIMO) techniques or re-configurable antennas [56]. The goal from using this equipment is to employ directional transmission and reception, since directionality is seen as a way of compensating the attenuation at high frequencies and, at the same time, limiting the interference [57] [58]. In this context, angle of arrival (AoA) and angle of departure (AoD) can be extracted from the signals exchanged between transmitter and receiver, which can be used for obtaining high accuracy ranging.

For example, in the mmWave case, given the directional nature of the communication, one requires node discovery and, hence, beam searching/steering capabilities [59]. This will involve gathering the parameters such as AoA from different directions. If the AoA is known from each of the ANs to the UE, then the UE´s location can be estimated using triangulation [60].

In Figure 8 we show a combined AoA – ToF approach. In this approach, the anchor node $\boldsymbol{A_1}$ estimates the azimuth angle, $\boldsymbol{\alpha_1}$, as well as the distance to the node with unknown position, $\boldsymbol{U}$. These two parameters, angle and distance, are enough for 2D position estimation of node $\boldsymbol{U}$. If 3D position estimation is required, the elevation angle (not shown in Figure 8) should be also estimated.

The estimation of these angles is performed using antenna arrays. For estimation of a single (azimuth) AoA, a linear antenna array can be used. Nevertheless, the estimation of both azimuth and elevation angles requires a more complex antenna array, e.g. rectangular. The distance estimation can then be performed using methods like TWR. Using this AoA – ToF approach, one anchor node with known position can be used for position estimation of other wireless nodes. This significantly reduces system complexity and relaxes the requirements for precise synchronisation between the nodes.

In the Sub-6 band, multi-antenna ANs are already available on the market. These ANs have already all required hardware for the AoA – ToF approach, hence it can be implemented in these ANs with minimal effort. In mmWave systems, achieving higher angular resolution requires antenna arrays with higher number of antenna elements, which is usually available given the reduced antenna size.

In summary, this method can greatly reduce the cost for installing indoor localisation systems, since the number of required devices (anchor nodes) is minimal and the required infrastructure (LAN) already exists.

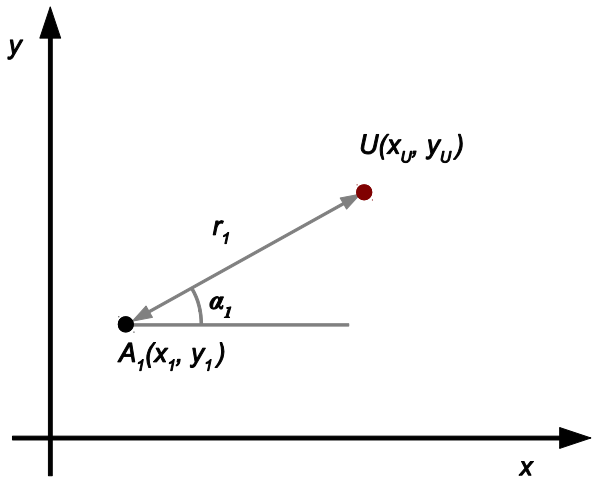

Figure 8: AoA – ToF combined approach for localisation.

2.2.1.2 Cooperative Localisation – Device-to-Device (D2D)

In cooperative localisation scenarios there is no infrastructure available. As shown in Figure 6b, the position of a node in the wireless network is estimated with respect to the positions of the other nodes [34]. This is a typical scenario for wireless sensor networks. Cooperative localisation methods based on time of flight measurements can be sensitive to clock frequency inaccuracy. Therefore, if no additional measures are taken, in indoor scenarios, the estimated distances can be significantly larger than the area of interest. Cooperative localisation methods are becoming interesting in 5G networks due to the envisioned device-to-device (D2D) functionality between the UEs.

In large wireless networks, the number of transmissions required for estimating the relative locations of the nodes can become significant, leading to an intensive use of the wireless medium. The **N-Way ranging method** is a cooperative positioning method that is able to reduce the number of transmissions needed to obtain the positions of all nodes in a wireless network [35].

In the basic form of the N-Way ranging method [35], it is assumed that all nodes in the network can communicate with each other. This is usually not the case in real scenarios, where not all nodes in a wireless network are visible to each other. Normally, the way forward is to search of smaller groups of nodes which can communicate with each other. The N-Way ranging can be performed between these groups and the results can be shared with the other neighbouring groups, and the relative locations of all nodes in the network can be estimated. If the locations of few nodes are known, the relative locations can be easily converted to absolute coordinates. This is why the N-Way ranging method can be either used in relative or in absolute positioning scenarios.

2.2.2 RF ranging methods

This section is devoted to give an overview of RF ranging methods used for estimation of the distance between two nodes.

2.2.2.1 Received Signal Strength (RSS)-based

It is a common approach to use the signal strength for localisation purposes in scenarios where the GPS signal is not available [32]. The extensive deployment of Wi-Fi networks, especially in indoor environments, has influenced the use of this signal feature, being the most commonly used method “Wi-Fi fingerprinting” [36]. This approach can offer good localisation precision but it is not robust to changes in the environment.

The main problem with RSS-based methods is that the received power decays fast for short distances between the wireless nodes and slowly for long distances. In addition, it is seriously affected by multipath propagation, leading to mismatches with respect to the theoretical expectations [37]. Figure 9 shows an example of the theoretical and the real dependency between received power and the distance between the nodes. It can be noticed that, due to fading (resulting from multipath propagation), the received power fluctuates around the theoretical value. There are no efficient methods that can be used to precisely estimate the distance as a function of received power in multipath propagation environments. Therefore, these methods cannot be used alone in localisation systems where centimetre level precision is required [38].

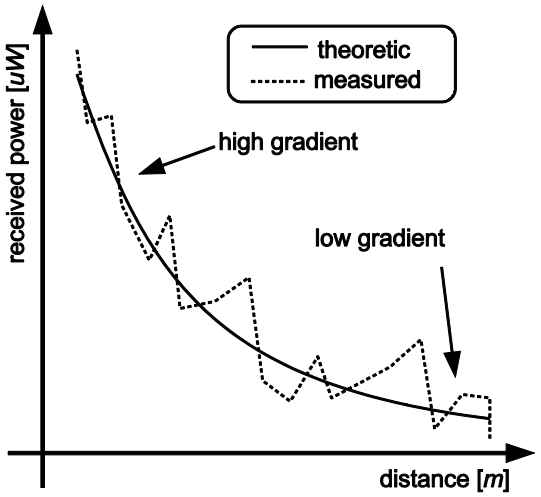

Figure 9: Received signal power as a function of distance between transmitter and receiver.

In terms of implementation, RSS-based ranging methods do not require additional hardware in the wireless nodes. The transceiver usually has a RSS circuit, which measures the received power level in order to perform signal conditioning (e.g. automatic gain control). The RSS information is also available to the user and is called Received Signal Strength Indicator (RSSI). This method can therefore be easily implemented in almost every wireless node.

2.2.2.2 Time-of-Flight (ToF)-based

The ToF based ranging methods exploit the RF wave propagation delay between two wireless nodes to estimate the distance. High ranging and localisation precision can be obtained using ToF-based methods. These methods exploit the finite propagation speed of the RF signal and are more suitable for use in multipath propagation environments [39]. However, their main drawback is the complexity of the hardware required, as well as the associated computational complexity. Obtaining high precision distance estimates with these methods in systems with limited resources is challenging. Precise distance estimation in NLoS scenarios can be also challenging. If the obstacle between the nodes only attenuates the waveform travelling the direct path, there is a direct path NLoS (DP-NLoS) scenario. In this case, ToF estimation with reduced precision is still possible. In case of non-direct path NLoS (NDP-NLoS), where the direct path is completely blocked and not arriving at the receiver, ToF estimation is not possible. In 5G networks, wireless nodes are expected to be densely distributed, which would minimize the probability for NDP-NLoS scenarios.

Time of Arrival (ToA) method

With this method, the ToA is estimated as a difference between the time of arrival and the time of transmission of a waveform (or frame). The ToA method is usually used in GNSS systems [40]. The main disadvantage is the requirement of high precision synchronised clocks in the nodes, which is challenging and costly. Different compensation methods are used in order to further improve the ranging precision and accuracy, which is limited by the achievable clock synchronisation precision and clock frequency inaccuracy at the nodes. Different methods for clock frequency inaccuracy compensation are listed in [40]. In any case, this method is usually avoided when providing ranging capabilities to low cost and low complexity devices.

Two Way Ranging (TWR) method

The most popular ToF-based distance estimation method is the TWR, being a common choice in indoor localisation applications. Two transmissions are needed to perform TWR, and only coarse or no synchronisation between the nodes is required. The required synchronisation precision is on the order of few microseconds [41], which is easily achievable.

Some implementations of the TWR method only require very relaxed synchronisation between the nodes. For example, [45] uses a special “burst mode” TWR approach, which prevents from tight synchronisation requirements. Another approach, presented in [47], uses a simple coarse synchroniser to detect the incoming ranging waveform.

3 Synchronisation Requirements for Small Cells

This chapter considers the requirements on synchronisation provision to small cells, and considers how these can be met when they are backhauled over wireless links. The toolbox of methods described in the previous chapter are assessed against the requirements. The wireless backhaul (BH) network elements themselves may need to be synchronised to communicate with each other, but this is not addressed here. However, it is clear that they can benefit from the same methods.

3.1 Synchronisation requirements from 5G

State-of-the-art wireless access networks, such as LTE-TDD, LTE Multimedia Broadcast Multicast Services (MBMS) and LTE-Advanced, have stricter frequency and phase synchronisation requirements compared to their predecessors, as shown in Table 2 [12]. Frequency synchronisation refers to the provision of a clock to a node whose periodicity is aligned to other nodes, whilst phase synchronisation implies that the phase or timing of the clock is also aligned. With the introduction of 5G, this requirement on clock provision will become tighter since 5G access will be more heterogeneous (requiring co-operation between different cells), will exploit unpaired spectrum in licensed and unlicensed bands – requiring Time Division Duplex (TDD) with framing alignment to minimise interference – and will exploit simulcasting to share common content to handsets.

Table 2: State-of-the-art synchronisation requirements for cellular access networks.

Cellular technology	Frequency requirement network/air	Phase accuracy	Note
LTE-TDD	16 ppb / 50 ppb	± 1.5 µs	Values for small cells (radius < 3 km)
LTE-MBMS	16 ppb / 50 ppb	± 10 µs	
LTE-Advanced	16 ppb / 50 ppb	± 1.5 µs to ± 5 µs	Depends on which LTE-A technology is used.

If we look beyond the access domain, wireless technologies are gaining increasing interest for FH and BH provision. Therefore, the operation of an efficient wireless transport network is likely to call upon similar methods to those developed for access, with corresponding synchronisation needs. Furthermore, the transport domain will be heterogeneous so there remains the need to propagate clocks across different wireless technologies (for example, mmWave using IEEE 802.11ad/ay [13] [14] and Sub-6 GHz using Wi-Fi or LTE TDD), and across optical technologies (such as WDM-PON).

3.2 Challenges and solutions

In this section, we restrict our focus to the challenges of providing clocks to small cells when the BH uses mmWave using IEEE 802.11ad/ay [13] [14]. The findings are also relevant to other similar wireless backhaul technologies, for example, those based on IEEE 802.11ac/ax. Clock delivery over wires (fibre, coaxial, etc.) is not addressed.

3.2.1 SyncE challenges

3.2.1.1 Network Architectures

Traditional microwave BH systems use fixed, high-gain dish antennae and are typically deployed in point-to-point configurations, where each modem in a transport node (TN) communicates with a single peer. In Figure 10, an arrangement of six TNs is drawn, a number of which are connected to one or more small cells. Each TN supports four independent modems, interconnected internally to the TN using a switch or router.

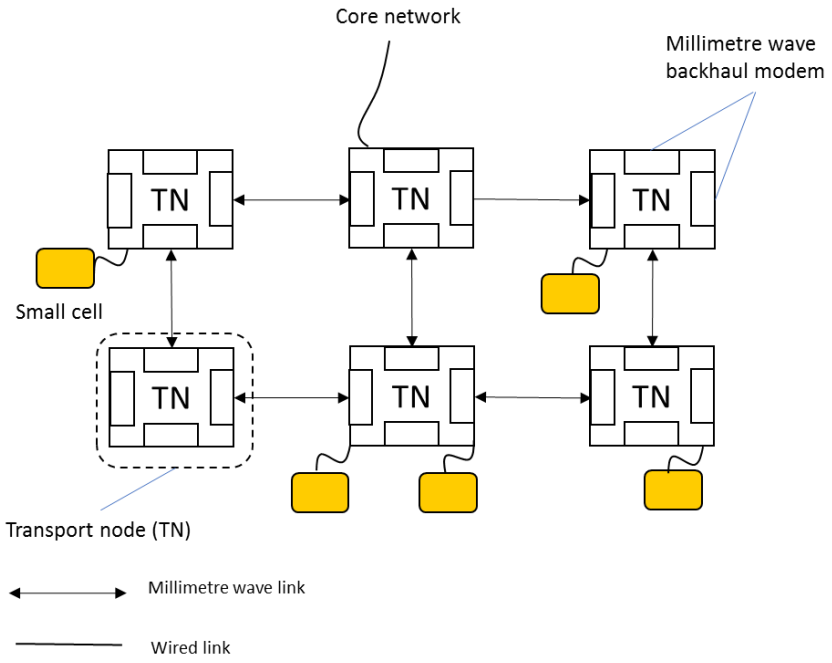

Figure 10: Point-to-point modem connectivity for wireless backhaul.

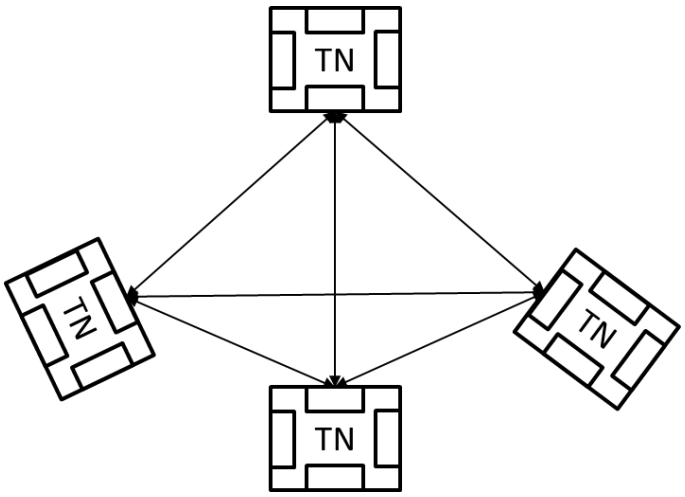

Figure 11: Point-to-multipoint configuration of mmWave interconnected TNs.

A mmWave TN can be built using low cost, electronically steerable, phased array antennae and can be used in a point-to-multipoint configuration. The point-to-multipoint networks are implemented using Time Division Multiple Access (TDMA) allowing a given modem in a TN to communicate with multiple peers, as depicted in Figure 11.

3.2.1.2 SyncE Distribution

The SyncE hierarchy is determined through the Ethernet Synchronisation Messaging Channel (ESMC) [29]. Each TN will have one slave interface and one or more master interfaces for propagation of the frequency through the network.

PTP SyncE Distribution

The slave peers recover the symbol rate of the master modem and use this to generate the downstream frequency for their other modems, Figure 12.

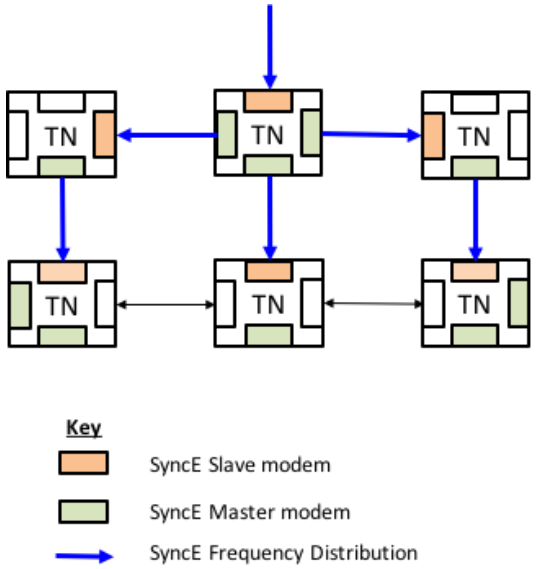

Figure 12: SyncE distribution for a point-to-point network.

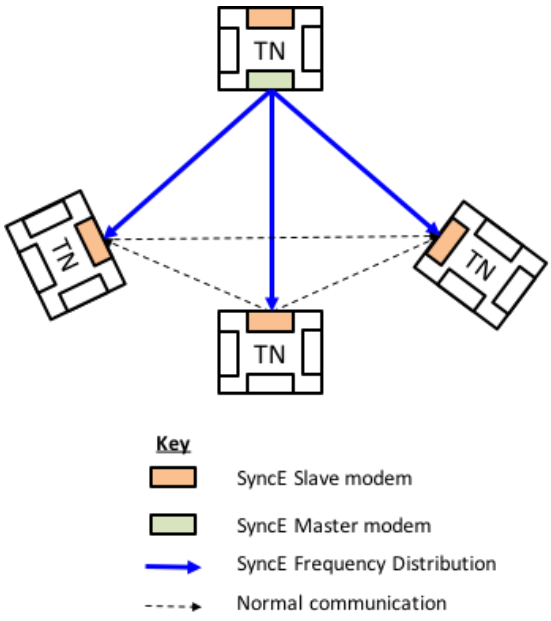

Figure 13: SyncE distribution for point-to-multipoint.

Point-to-Multipoint SyncE Distribution

In a point-to-multipoint network, a given modem may be capable of communicating with multiple peers. SyncE distribution paths are shown in Figure 13.

SyncE distribution per TDMA slot is shown in Figure 14. In the slots marked for SyncE frequency distribution there is a regular data transmission, but since the master is transmitting an accurate clock can be recovered using SyncE.

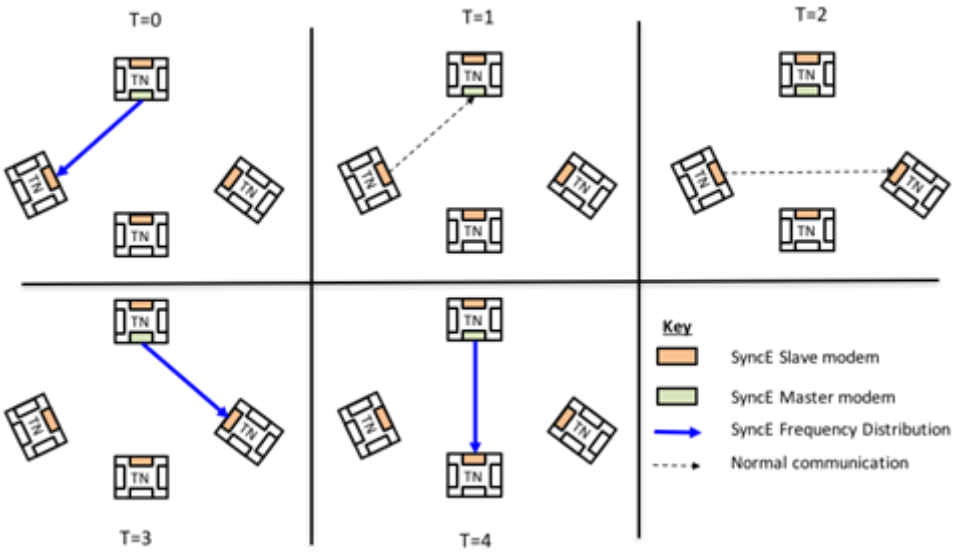

Figure 14: SyncE distribution per TDMA slot.

Some implications are:

A. There is not a constant signal from which the SyncE frequency can be extracted.
B. Packets are being received from both the SyncE master modem as well as other slave modems.
C. The timing of packet reception from the SyncE master may be non-deterministic.

The low cost TDD radio devices used in mmWave TN means that:

D. The same clock signal is used for transmission and reception in the radio.

A potential solution that addresses these needs is now described, and is shown in Figure 15. The baseband (BB) estimates the carrier frequency offset (CFO) between the input frequency to the radio and the frequency used at the transmitter as well as capturing the time of arrival (ToA) for every packet received. The tuple *{CFO, ToA}* is passed to the Medium Access Control (MAC) layer.

The MAC layer has been configured to know the MAC address of the modem from which the SyncE clock signal is to be extracted. The tuple *{CFO, ToA}* for each packet received from the master modem is passed to a software application running a filter. The filter application adjusts the input frequencies used by all modems to track that of the master. The adjustment is performed slowly enough to avoid needing synchronisation with an idle time at the node.

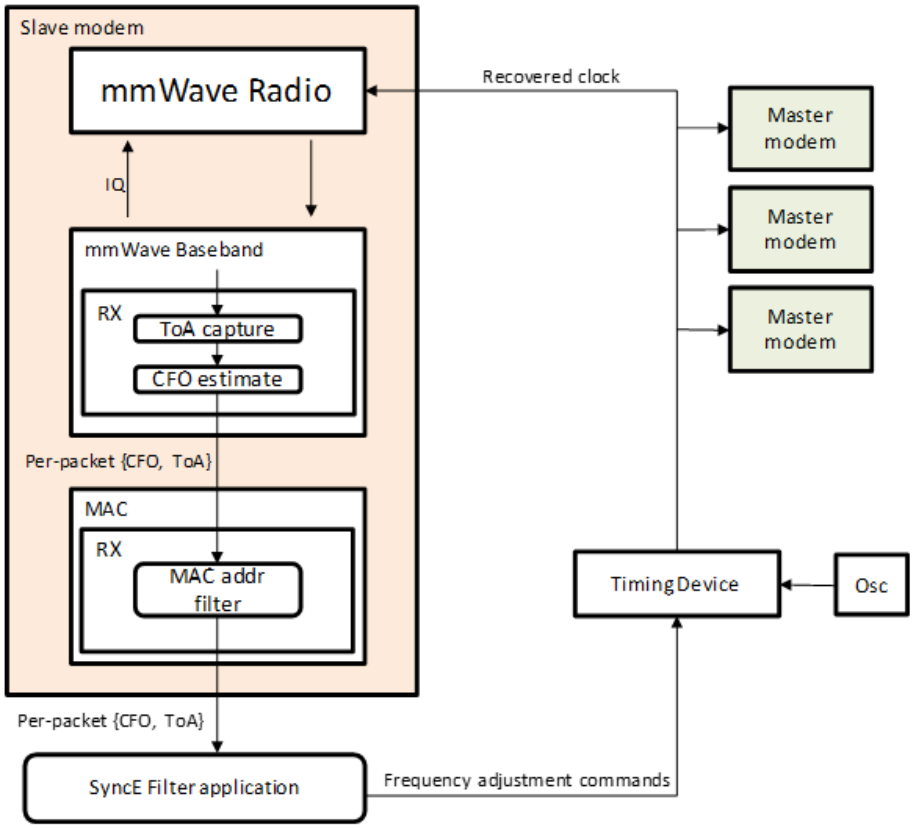

Figure 15: SyncE clock recovery architecture in a mmWave modem of a 4-modem TN.

How does this address the constraints, A-D above?

A. No constant signal
   - The clock must not be derived directly from a clock output pin from the modem: the modem must provide frequency offset reports to a local process.
   - The controlling modem where the scheduler lies – e.g. the Personal Basic Service Set (PBSS) Control Point in IEEE 802.11ad) must ensure that the master modem transmits to all slaves at least as frequently as the hold-over duration.
   - The TN must be capable of high quality hold-over (able to run with drifting too much when the synchronisation adjustment is not available).

B. Reception from multiple modems
   - The process must discriminate between modems when recovering frequency.

C. Non-deterministic sync events
   - The process must understand the time relationship between the frequency offset reports from the modem.

D. Frequency adjustment is performed within the tolerance of the radio
   - The process must make small adjustments so that communication is not interrupted.

3.2.2 IEEE 1588 challenges

An example of an implementation of IEEE 1588v2 over a wireless backhaul (BH) mesh is shown in Figure 16. In the example, the BH operates at 60 GHz, with each transport node comprising 60 GHz modems and a Network Processing Unit (NPU) board to switch traffic and provide ancillary functions. Wireless BH technologies using IEEE 802.11ad or Wi-Fi have limited range of a few hundred metres. Additionally, IEEE 802.11ad relies upon LoS links so extra hops may be needed to route BH traffic around buildings and obstacles. Consequently, there can be a number of wireless hops which poses challenges for point-to-point given that every intermediate node adds to the inaccuracy of the correction field (residence time).

For each wireless, node there is a choice of implementing BCLs, or TCLs. TCLs require fewer 1588 protocol stacks potentially reducing the cost of the TN. TCLs can participate in the delay request-response mechanism, and include the ToF of the wireless link into the residence time estimate.

Another challenge is that the wireless medium is shared in the time domain (TDD/TDMA), so transmission of PTP event messages are unlikely to be at regular intervals unless measures are taken such as giving isochronous slots. This is not problematic if there is an alternative source of synchronisation (e.g. SyncE). Accuracy of time stamps may be improved by sending event messages over the air interface on their own without aggregation with other packets or management frames, and using a transmission rate that is invariant (fixed modulation and coding scheme). SyncE should be provided (because frequency synchronisation from PTP alone is not sufficiently accurate – see discussion above), and this can be used to clock the time stampers in the transport node devices (for example, there could be a time-stamper in each modem and the NPU). Additionally, a pulse per second (PPS) signal should be used to start time stampers at the same instant of time.

PTP event messages are recognised on arrival from a unique MAC address. The time of arrival at the transport node (taken to be some point in the physical reception, such as the preamble with correction for additional time for the last byte of the message itself) is time stamped. The exit time stamp is calculated as the time when the packet goes on the medium. Since time stamping is performed in the MAC, correction for the time from leaving the MAC to the first byte going on the air must be added. Note that, although that time is bounded (under normal conditions), in contention-based MAC (such as in IEEE 802.11ac/ax), its value is completely random. However, studies like [26] argue that sub-1 µs precision can be achieved with software timestamping and appropriate adaptation of the IEEE 1588.

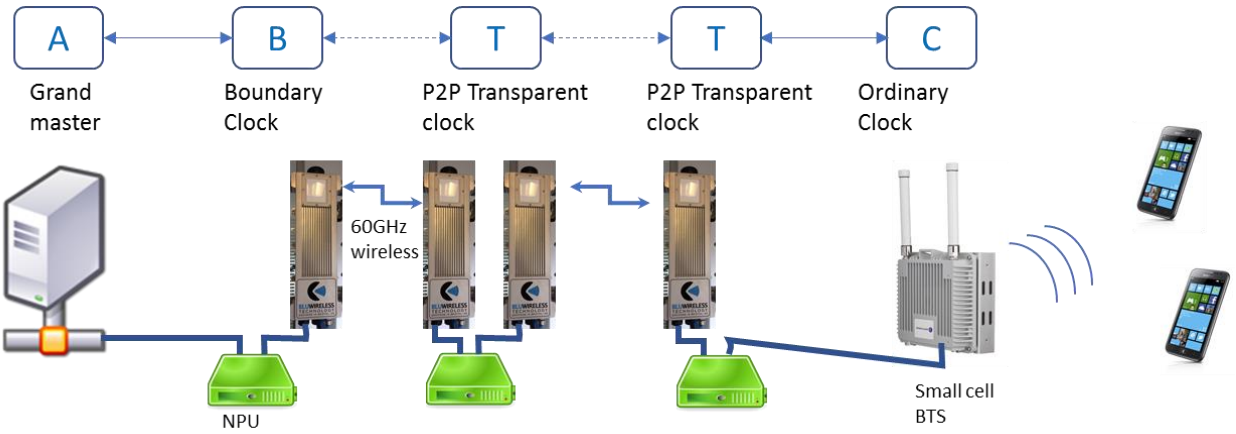

Figure 16: Backhaul from a small cell over wireless hops with clock hierarchy.

4 Localisation and ranging: algorithms and implementation

In the 5G-XHaul project we investigate ranging methods that can be used for positioning estimation using trilateration, being these methods suitable for implementation in wireless nodes present in, for example, dense urban scenarios. The main focus is on methods which can be used either in Sub-6 GHz systems as well as in 60 GHz systems, which are the wireless technologies being considered in 5G-XHaul.

For the Sub-6 bands, we have developed RF ranging systems which can be used for positioning applications, e.g. using trilateration. The main goal is to investigate the achievable ranging precision in the Sub-6 bands. We use a software defined radio (SDR) platform for implementation and testing of the ranging methods.

In the 60 GHz band we evaluate the ranging precision using commercial off-the-shelf (COTS) equipment. The acquired data is processed in software on a host computer to perform ToF and, as a result, we can estimate the distance.

4.1 Algorithms used for ranging

In 5G-XHaul we consider ranging methods based on ToF estimation for precise ranging. The two most common methods used for ToF estimation are ToA and TWR. The time diagrams of these methods are shown in Figure 17.

If ToA ranging is performed, both stations, ***N₁*** and ***N₂***, are synchronised. The station ***N₁*** transmits a frame to station ***N₂*** at a time instant agreed between the stations. The station ***N₂*** receives this frame after the ToF and estimates the ToA. Having the time of transmission at ***N₁*** and time-of-arrival at ***N₂***, the ToF can be easily estimated.

In the case of TWR, a frame is transmitted from ***N₁*** to ***N₂*** and further ***N₂*** replies to ***N₁*** with a new frame. Both station estimate the ToA of the received frames. Station ***N₁*** estimates also the round-trip-time (RTT) as a difference between the time of arrival and the time of transmission. Station ***N₂*** estimates the reply time as a difference between the time of transmission and the time of arrival. Having the RTT and the reply time, the ToF and, therefore, distance can be easily estimated.

In both methods, time of arrival of a frame must be precisely estimated. Pulse compression techniques [49] with phase coded waveforms are a common choice if ranging (or localisation), i.e. time of arrival estimation, should be implemented in wireless data transceivers. The phase coded waveforms are obtained by modulation of a pseudo-noise (PN) sequence using a phase (BPSK, QPSK, etc.) modulation. The pulse compression is achieved by cross-correlating the received waveform with a locally generated copy of the same sequence. The output of the correlator would produce a narrow peak which position is the time of arrival of the received waveform.

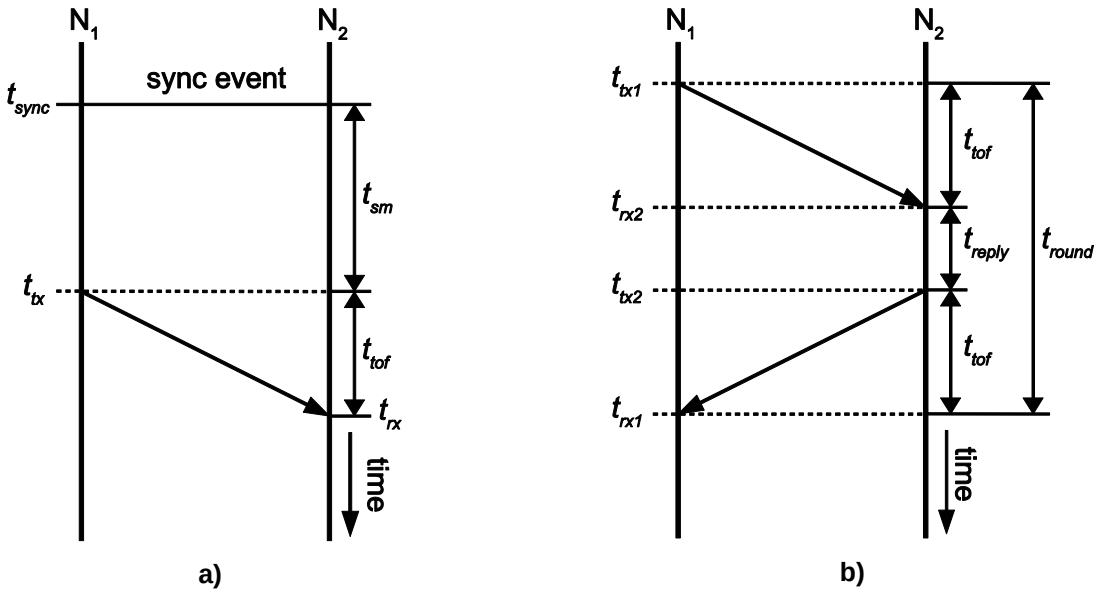

Figure 17: Timing diagrams of different ranging methods, a) ToA, b) TWR.

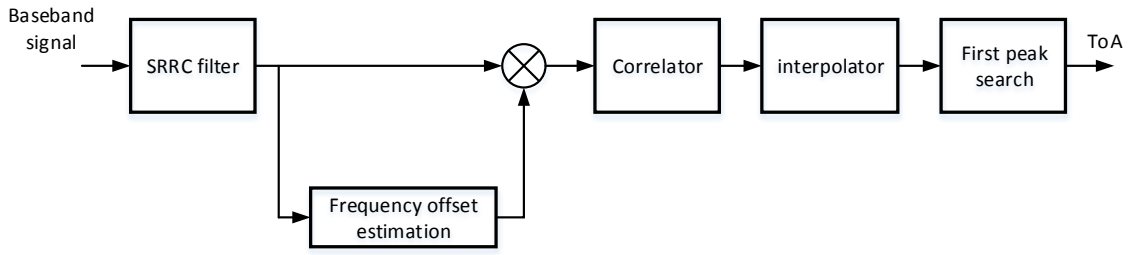

Figure 18: Block diagram of the time of arrival estimator.

In Figure 18 a simple time of arrival estimator is shown. This basic ToA estimator can perform a subsample precision ToA estimation. Other types of estimators can be found in [61][62].

This estimator filters the received signal using square-root-raised-cosine filter (SRRC) filter and corrects the frequency offset before performing cross-correlation. In order to acquire a subsample precision ToA estimation, it interpolates the obtained cross-correlation function. The ToA estimation is achieved by searching for the position of the first peak in the cross-correlation function.

4.2 Ranging in the Sub-6 band

The ranging system developed in 5G-XHaul uses the 2.4 GHz ISM band, since no additional licenses are needed if certain limits regarding the irradiated power are complied [67]. This system is running on a SDR platform and the implementation is performed in software. The software implementation requires less effort compared to hardware implementation and at the same time offers greater flexibility for adding future changes and functionalities. Nevertheless, achieving performances that the hardware system would have is challenging. On one hand this simplifies the implementation compared to pure hardware implementation but, on the other hand, different issues associated with pure software implementation should be considered and solved.

4.2.1 The software defined radio (SDR) platform

The ranging system developed in 5G-XHaul is implemented on a SDR platform from Ettus Research [48]. Two models, namely N210 and B205mini-i, are used for this implementation. The main specifications of the two radios are shown in Table 3 and Table 5, respectively. The Ettus Research N210 model requires a separate analogue front-end (AFE). For the implementation and testing, the SBX AFE from Ettus Research is used. Its main specifications are given in Table 4.

Table 3: Main specifications of the SDR radio N210.

Parameter	Value
SDR model	Ettus Research N210
Connection to host computer	1 Gbps Ethernet
A/D resolution	14-bit
A/D sample rate	at host computer: 50 MSps – 8-bit samples <=25MSps – 14-bit samples internally at SDR: 100 MSps – 14-bit samples
D/A resolution	16-bit
D/A sample rate	at host computer: 50 MSps – 8-bit samples <=25MSps – 16-bit samples internally at SDR: 400 MSps – 16-bit samples
DUC/DDC tuning resolution	25 MHz
Frequency accuracy	2.5 ppm (TCXO) 0.01 ppm (with GPSDO option installed)

Table 4: Main specifications of the SBX AFE.

Parameter	Value
AFE model	SBX 400 – 4400, RX/TX (40 MHz)
Output power	100 mW
Typical noise figure	5 dB
Frequency range	400 – 4400 MHz
Bandwidth	40 MHz
Transmit gain range	0-31.5 dB
Receive gain range	0-31.5 dB

Table 5: Main specifications of the Ettus Research B2015mini.

Parameter	Value
SDR model	USRP B205mini-i
Connection to host computer	USB 3.0
A/D resolution	12-bit
A/D sample rate	61.44 MSps – 12-bit samples
D/A resolution	12-bit
D/A sample rate	61.44 MSps – 12-bit samples
DUC/DDC tuning resolution	25 MHz
Frequency accuracy	2 ppm 0.01 ppm (with GPSDO option installed)
Power output	>10 dBm
Receive noise figure	<8 dB
Frequency range	70 – 6000 MHz
Bandwidth	up to 56 MHz

The model B205mini-I, on the other hand, has integrated AFE which covers the frequencies 70-6000 MHz. A simplified block diagram of the SDR platform is shown in Figure 19. The received waveform is down-converted and sampled using the A/D converter. These samples are time stamped and sent to the host computer using a Gigabit Ethernet or USB 3.0 connection. The samples to be transmitted are transferred to the SDR platform using the same connection. They can be also time stamped. The digital samples are converted to the analogue domain using the D/A converter and transmitted using the AFE. The AFE has two mixers, used for up-conversion and down-conversion of the BB signal. Nevertheless, the frequency resolution of the local oscillator used for up-conversion and down-conversion is not high enough and, therefore, a digital down-converter (DDC) and digital up-converter (DUC) are used in the SDR platform for fine-tuning of the carrier frequency. With this approach a carrier frequency tuning precision of 25 millihertz can be achieved.

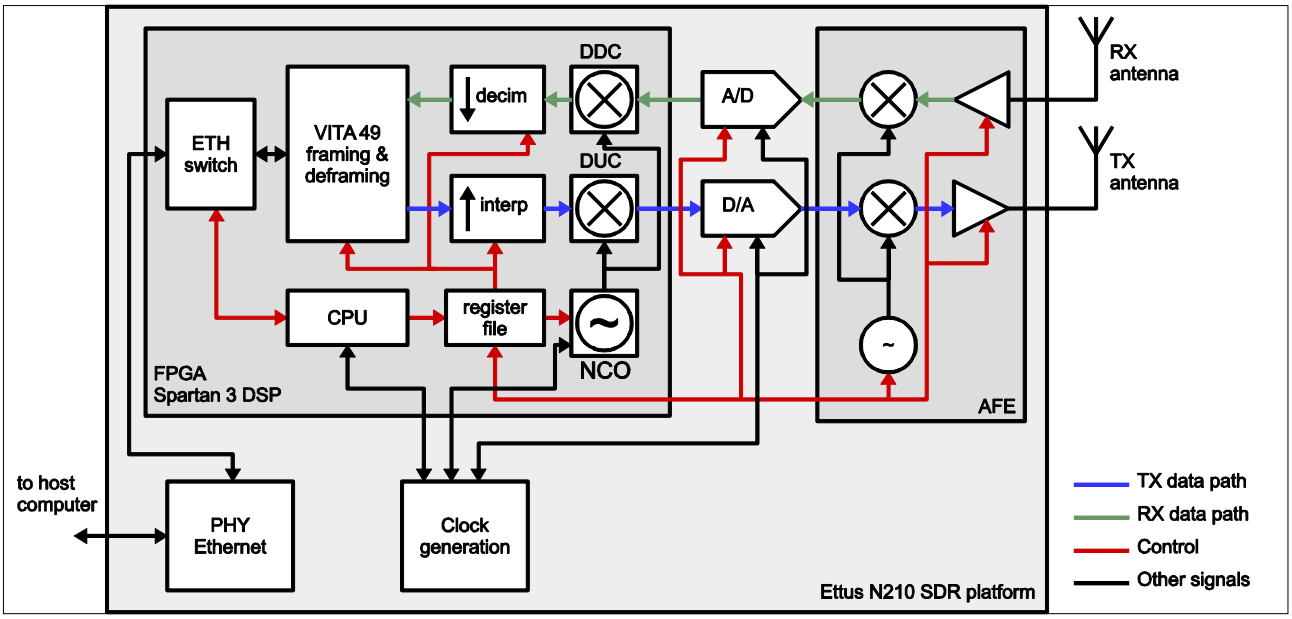

Figure 19: Simplified block diagram of the SDR platform [48].

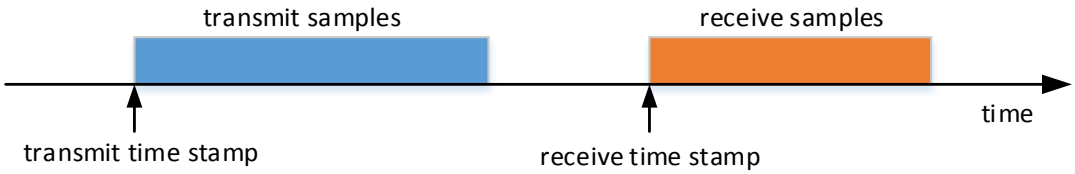

Figure 20: SDR time stamping functionality.

An important functionality of these SDR platforms is the support for time stamping of the transmitted and received samples. This is important for ranging applications since precise measurement of time intervals is essential for time-of-flight (ToF) and, therefore, distances estimation. The time stamping functionality is illustrated in Figure 20. The samples to be transmitted are associated with a transmit time stamp and transferred to the SDR platform. When the internal clock of the SDR platform becomes equal to the transmit timestamp, the samples are transmitted. In order to receive samples, the host computer issues a time stamp to the SDR platform for the time when the samples should be acquired. Also, the number of samples to be transmitted is supplied to the SDR platform. When the internal timer of the SDR platform becomes equal to the receive time stamp, the specified number of samples are acquired and transferred to the host computer.

The SDR platforms can also support continuous acquisition/transmission of samples. Nevertheless, for higher sample rates (more than a couple of tens of MSps) huge computational resources for signal processing would be needed and, therefore, this mode is avoided in ranging applications.

4.2.2 Two way ranging (TWR) implementation using a SDR platform

The TWR method described in Section 4.1 can be implemented on a SDR platform using two different approaches. The first approach is to continuously process the incoming samples and to detect an incoming frame used for ranging. When this frame is received a new frame is sent back. This approach is presented in Figure 17b. The main problem with this approach is the huge computational power required for processing of the incoming samples. Therefore, in order to perform the TWR this approach must be, at least partially, implemented in hardware. The second approach is to perform the TWR approach in time windows scheduled in advance. A method for synchronisation of these time windows is developed here in order to test and evaluate TWR.

Implementation of the TWR method using time windows

The time diagram of the TWR method implemented in this work is shown in Figure 21. Station ***A*** schedules samples for transmission and a time window for reception. The same is performed in station ***B***, who schedules a time window for reception and the number of samples to be transmitted. Both the frame and the reception time window are scheduled using the time stamping feature of the SDRs. For the frame to be transmitted, the developed software supplies the time stamp as well as the ranging frame to the radio. Subsequently, for the reception window, the software supplies a time stamp to the SDR and obtains the samples acquired, starting from the time specified in the time stamp. The acquired samples from both receive windows are then used for time-of-flight (ToF) estimation.

Synchronisation of the ranging windows in both stations

To implement the TWR on the SDR platforms using the approach described, both SDR platforms, i.e. wireless stations, should be synchronised. This synchronisation can be performed in two different ways. First, a wired connection can be used between the two stations. This solution is not favoured since, in realistic localisation scenarios, many cables would be needed and the deployment area size would be limited by the cable lengths. The second possibility is to use wireless synchronisation between the nodes. In 5G-XHaul, we propose a method that can be used for synchronisation between the wireless nodes in order to perform TWR, which is shown in Figure 22.

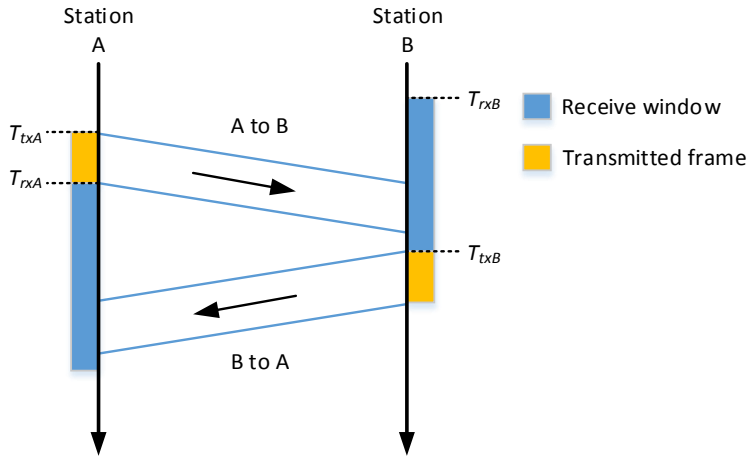

Figure 21: TWR implemented on the SDR platform using the time stamping functionality.

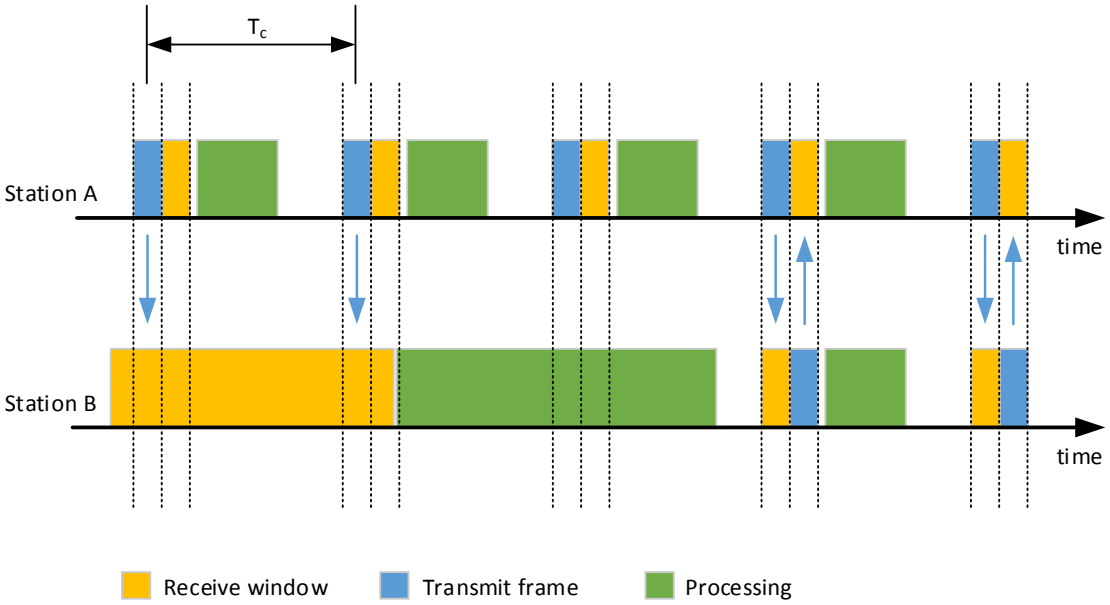

Figure 22: Synchronisation between two devices before performing TWR.

In the proposed method, one of the stations, in this case station ***A*** is the master, and the other, station ***B***, is the slave. When station ***A*** is powered up, it starts transmitting ranging frames periodically with a period of T_C. When the station ***B*** is powered up, it acquires samples for a period longer than T_C. This is needed in order to ensure that at least one complete ranging frame from station ***A*** would is acquired station ***B***. Station ***B*** processes the acquired samples to estimate the time of arrival (ToA), i.e. time of reception, of the ranging frames from the station ***A***. When the ToA is estimated, node ***B*** predicts the time of the next transmission of station ***A*** and schedules a reception window. In addition, a ranging frame to be transmitted from station ***B*** is scheduled after the receiving window. This frame should be received in station ***A***, who schedules a receive window. As can be seen in Figure 22, after the initial synchronisation phase, the TWR is performed between the two stations periodically with a period of T_C.

Due to the clock frequency offset present in both stations, it might occur that receive windows are not synchronised with the frame transmissions as shown in Figure 23. In this case, station ***B*** would not receive the frame from station ***A***, and station ***A*** would not receive the frame from station ***B***. The TWR would not be performed correctly and, therefore, the distance between the nodes would not be properly estimated. This can be corrected by resynchronising the nodes in the same manner as it was performed on power up. Nevertheless, this is time consuming due to the need for processing of large amount of acquired samples.

In our case, we perform a re-synchronisation each time a frame is received. Therefore, if the receive window in station ***B*** is slightly shifted with respect to the transmitted frame from station ***A***, this shift would be immediately corrected. This procedure prevents from accumulating timing errors and, in addition, a power up synchronisation procedure would not be necessary. This power up re-synchronisation procedure would only be needed if no frame is received in multiple successive receive time windows.

The TWR between the stations in this implementation is performed periodically with a period of T_C, in order to simplify its implementation. Nevertheless, this must not be the case. The stations, once synchronised, can negotiate a new value for the time T_C and change it for each next TWR.

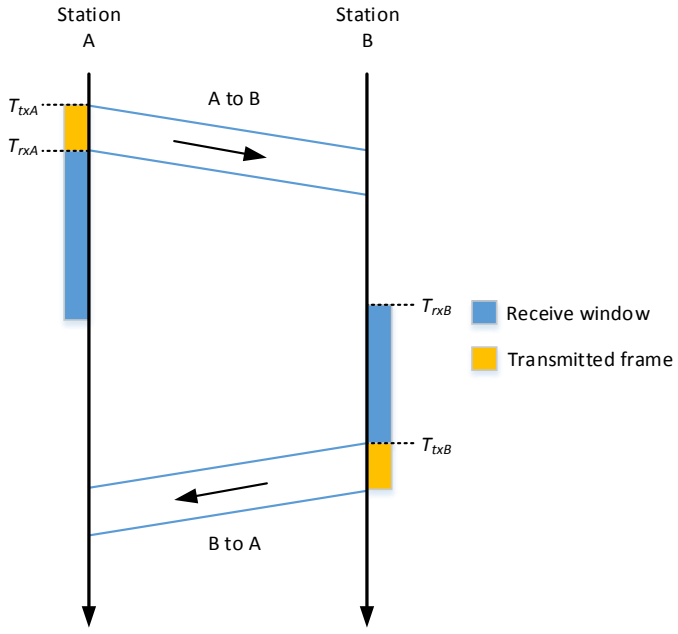

Figure 23: TWR between two stations which are not synchronised.

ToF estimation

Time-of-arrival (ToA) estimation of the ranging frames must be first performed to then estimate the distance. The ToA is estimated with respect to the receive time stamp, T_{rxA} or T_{rxB}. The transmitted ranging frame is time stamped using the same time reference as the received samples and, therefore, the ToA with respect to the transmit time stamp, T_{txA} or T_{txB}, can be easily calculated (see Figure 24). In station ***A***, the ToA estimated with respect to the time stamp of the transmitted frame represents the RTT and, in station ***B***, it represents the reply time. The availability of both RTT and reply times allows the calculation of the ToF and, as a result, the calculation of the distance. The estimator shown in Figure 18 is used for ToA estimation in this approach.

State machine of the nodes – master and slave

In our implementation, two SDR stations are used to perform ranging, one acting as the master and the other as the slave. Both stations are being controlled by finite state machines (FSMs) given in Figure 25.

The master station starts by transmitting a frame (*state 2*) and receiving a given number of samples immediately after the transmission (*state 3*). The received samples are processed (*state 4*) and, if a ranging frame is received, the reply time estimate is transmitted to the slave station with the next ranging frame.

The slave, on the other hand, must synchronize to the transmissions from the master. Therefore, on power-on, the slave acquires samples from the received signal for a period of time T_C (*state 2*). These samples are processed (*state 3*) in order to find the frames being transmitted from the master. If no frames are found, a new set of samples is acquired (*state 2*). In case a frame is found, a reception (*state 4*) and transmission (*state 5*) are scheduled in order to receive the next transmission of the master and to transmit a frame back to it. The received samples are processed and the reply time is estimated and transmitted back to the master node using the next transmission. Finally, the master estimates the ToF and transmits it to the slave.

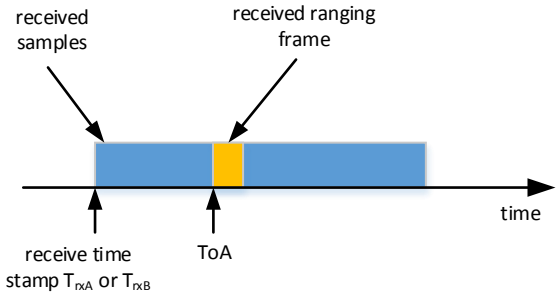

Figure 24: Received ranging frame falling into the samples acquired in the receive window.

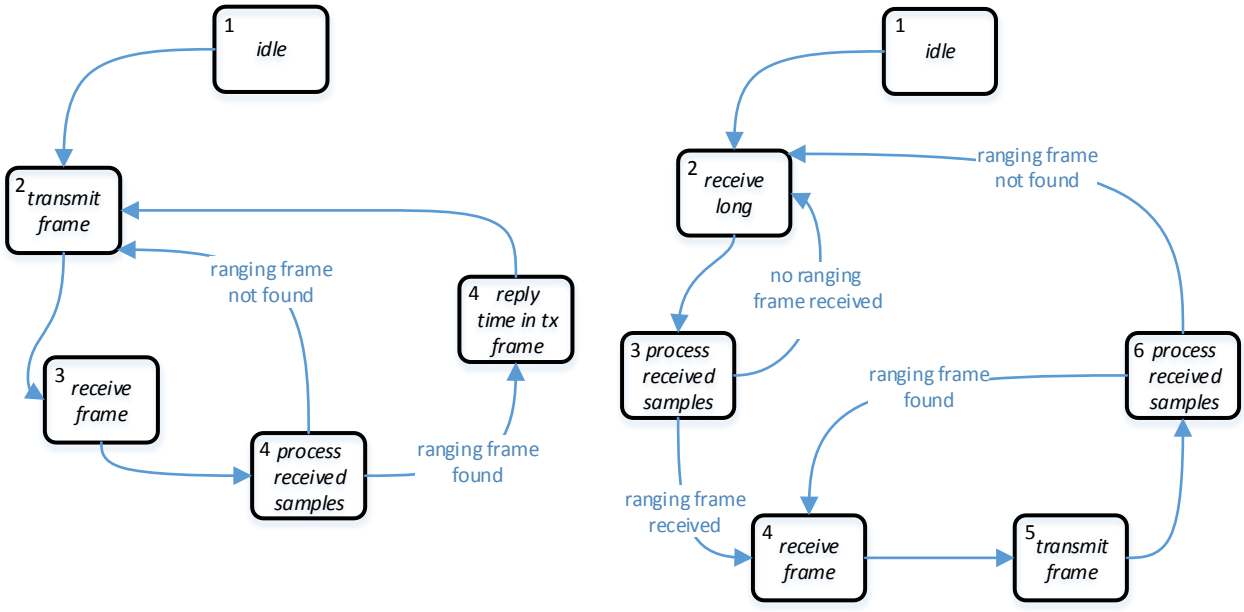

Figure 25: FSM for controlling the master station (left); FSM for controlling the slave station (right).

Figure 26: Frame used for ranging.

Table 6: Structure and bits of the header used for ranging.

Field	Width [bits]
Source address	16
Destination address	16
Frame type	8
Data Length	16
Sequence number	16
PN sequence length	16
PN sequence type	8
Position (X)	32
Position (Y)	32
Position (Z)	32
Reply time	32
Time of flight	32
CRC16	16

The structure of the frame used for ranging is shown in Figure 26, and consists of a preamble, a header and a ranging sequence. Short guard intervals of 32 zero samples are inserted between the preamble and the header, as well as between the header and the ranging sequence (not shown in Figure 26). This frame is modulated using BPSK modulation.

The **preamble** consists of eight copies of the short training symbols (STS) used in WLAN (802.11a) [50]. This preamble is used for detection of the arriving frame and for frequency offset estimation. Its duration is different compared to that of WLAN since they use different sample rates. Due to the different lengths of the STS symbols, the WLAN frames are not mixed up with the used ranging frames.

The **header** is used to transfer the necessary data between the two stations. The fields of the header are given in Table 6.

The **PN sequence** is a maximum length sequence (MLS) or m-sequence generated using the polynomial $x^{10}+x^3+x^2+1$, being the initial state of the shift register set to all ones. The bits of the m-sequence are modulated using BPSK modulation.

Measurement campaign

The implemented Sub-6 system was tested in order to assess the achievable ranging precision. The system was evaluated using two different antennas. For the first set of measurements, a 2.5 dBi omnidirectional antenna was used. The second set of measurements was performed using a patch antenna with 6 dBi gain. In each station, the same antenna was used as receive and transmit antenna, since the stations are working in TDD mode. The system was tested in an anechoic chamber as well as in a hallway under more realistic conditions.

The anechoic chamber has dimensions 7 m x 4 m x 2.2 m, and is intended for frequencies from 1 GHz up to 100 GHz. The evaluation is performed on a frequency of 2.45 GHz in the ISM band. The transmit power is controlled dynamically to achieve good coverage of the dynamic range of the A/D converter at the receiver. Nevertheless, the maximum transmit power is limited to 15 dBm. The distance between the master and the slave station is changed from 1 to 5.4 metres due to the physical limitations of the anechoic chamber. A sketch of the anechoic chamber is given in Figure 27. For each distance, a couple of hundreds of measurements are performed in order to extract the probability distribution of the estimated distance. The first measurements were performed using omnidirectional antennas.

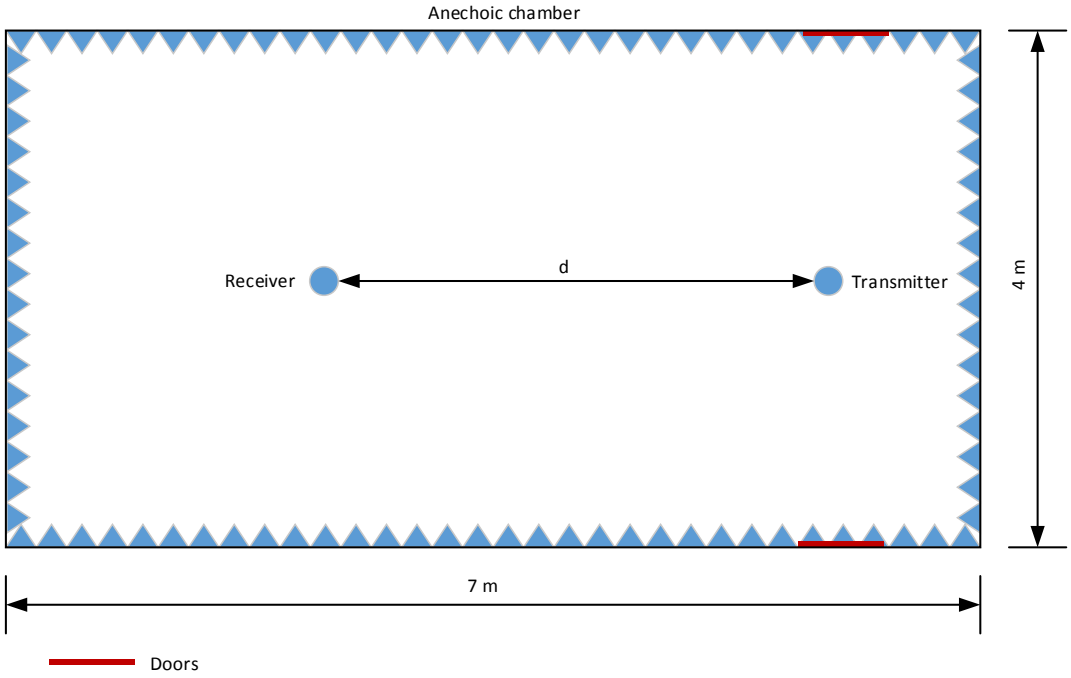

Figure 27: Sketch of the anechoic chamber used for the measurement campaign.

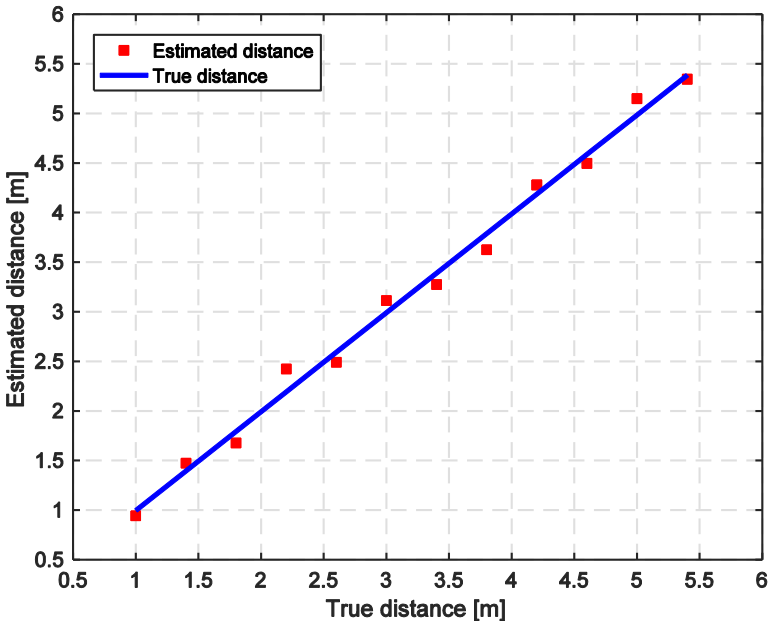

Figure 28: Estimated distance VS true distance (anechoic chamber; omnidirectional antennas).

The mean values of the estimated positions, compared to the true positions are shown in Figure 28. The root mean square error (RMSE) of the measurements for each position with respect to the true position is represented in Figure 29.

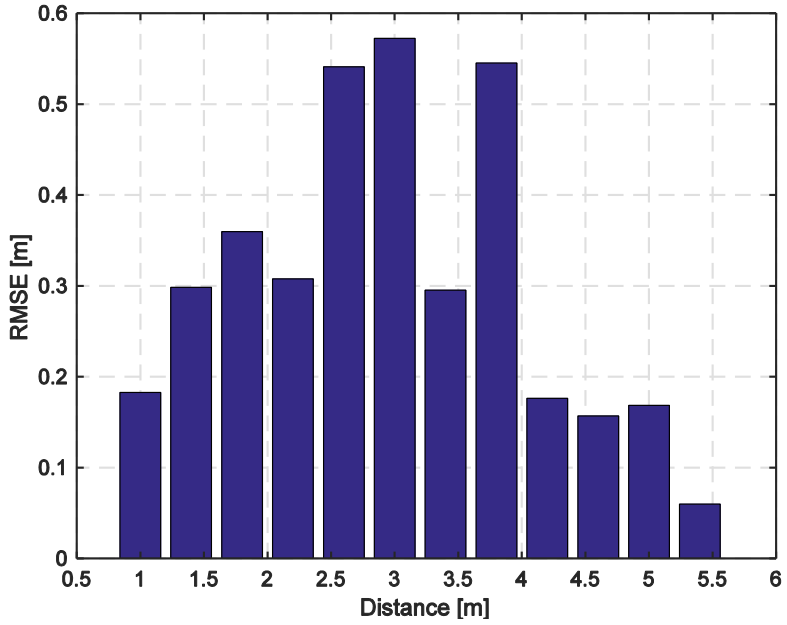

Figure 29: RMSE as a function of distance (anechoic chamber, omnidirectional antennas).

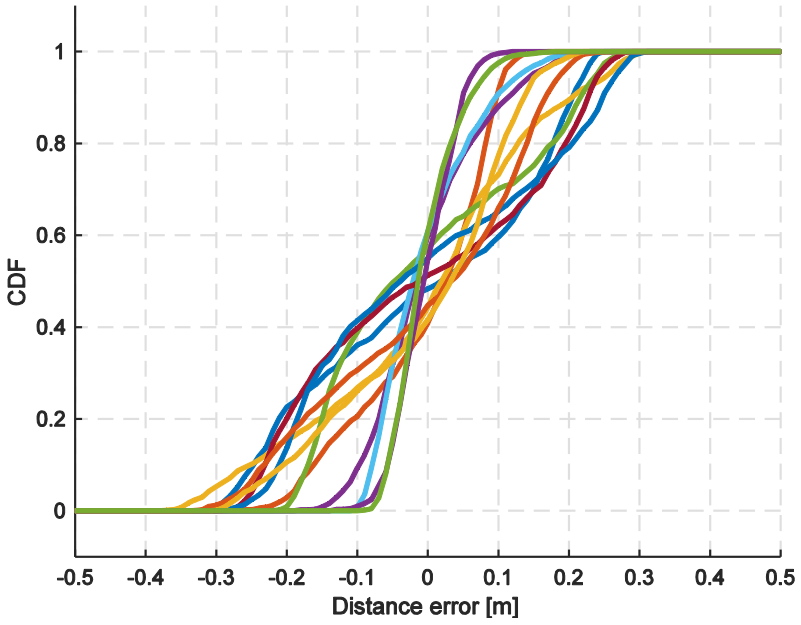

Figure 30: CDF of the estimation error for all distances (anechoic chamber; omnidirectional antennas).

It can be noticed that the maximum RMSE is less than 0.5 metres. For these measurements, the cumulative distribution function (CDF) of the error for each distance is given in Figure 30. Each line corresponds to a different distance starting from the smallest to the largest. The CDF gives better insight of the distribution of the estimation error. It represents how the noise and the imperfections of the radio system affect the distance estimation error. The CDFs in Figure 30 are calculated with respect to the mean estimated value, and not to the true distance. It can be seen that the estimates are dispersed in the interval of ± 0.3 metres around the mean value

The same measurements were repeated using **patch antennas** with an antenna gain of 6 dBi. The distance estimates compared to the true distances, in this case, are given in Figure 31.

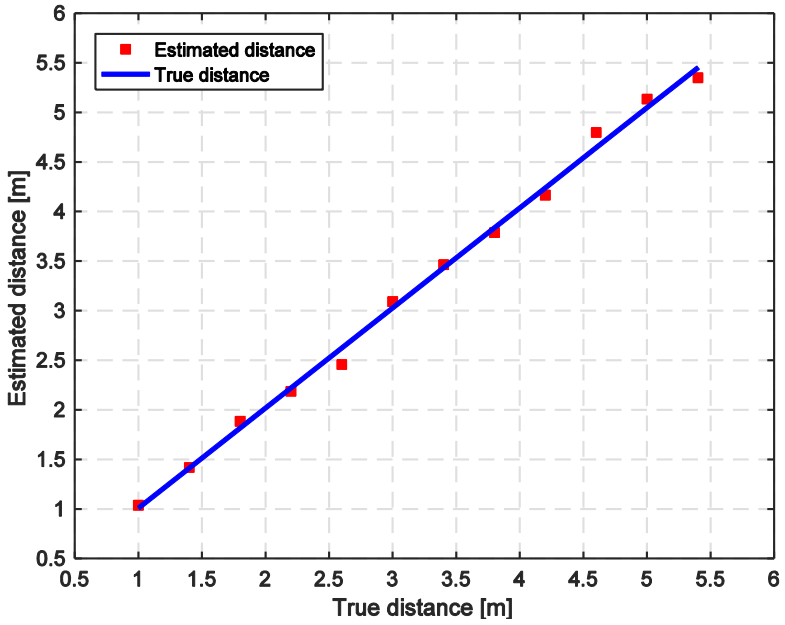

Figure 31: Estimated distance VS true distance (anechoic chamber, 6 dBi patch antennas).

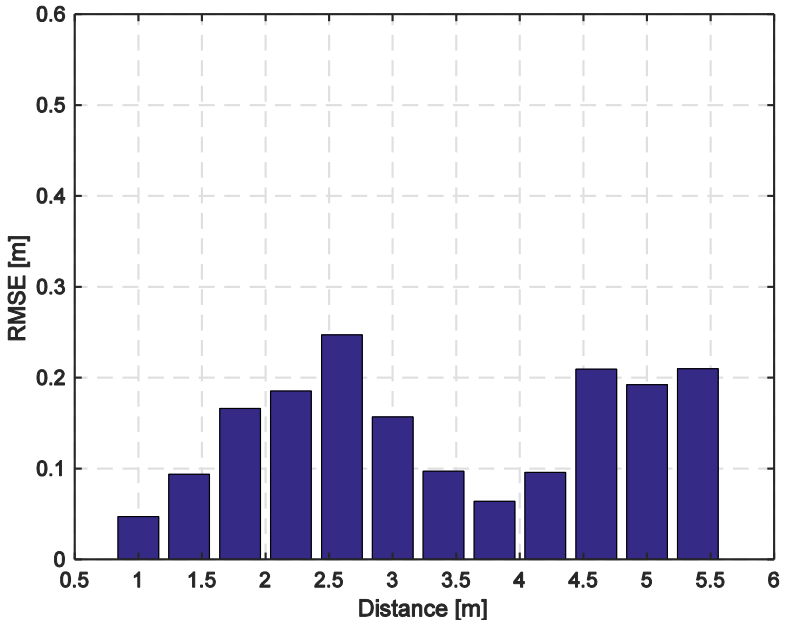

Figure 32: RMSE as a function of distance (anechoic chamber; 6 dBi patch antennas).

The RMSE as a function of distance is given in Figure 32. It can be noticed that the error is slightly lower compared to the case with omnidirectional antennas. In this case, the distance estimation error is less than 0.3 metres and is basically half the ranging error compared to the case when omnidirectional antennas are used. The reason for the better accuracy is the imperfection of the anechoic chamber. The reflections in the anechoic chamber are minimal, but due to the equipment and the cables used to perform the measurements, these reflections would not be negligible in ranging and positioning applications.

The CDFs for each distance estimate are plotted in Figure 33. They are calculated with respect to the mean distance estimate. The plots are very similar to the ones in Figure 30. As expected, in a static scenario, the results should not depend on the reflections and, therefore, when using either omnidirectional or patch antennas, we obtain almost the same distributions.

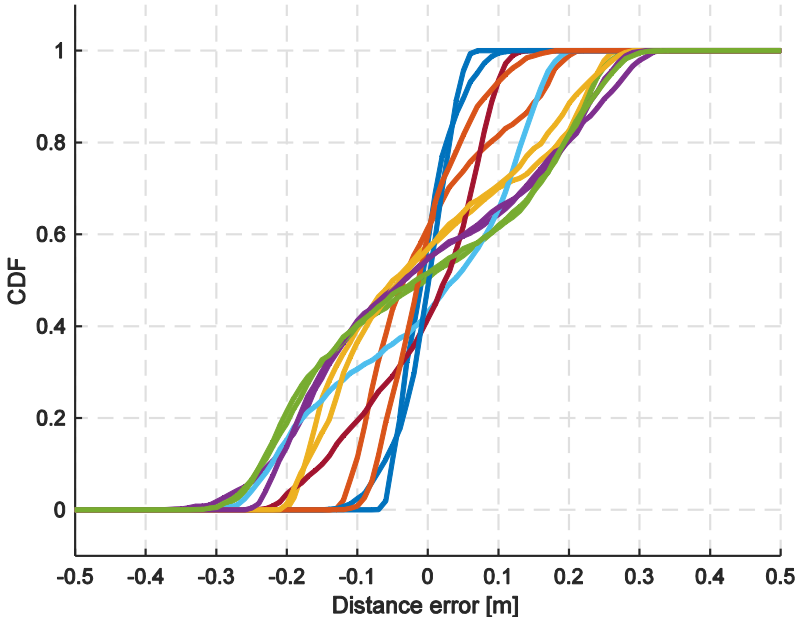

Figure 33: CDF of the estimation error for all of the distances (anechoic chamber; patch antennas).

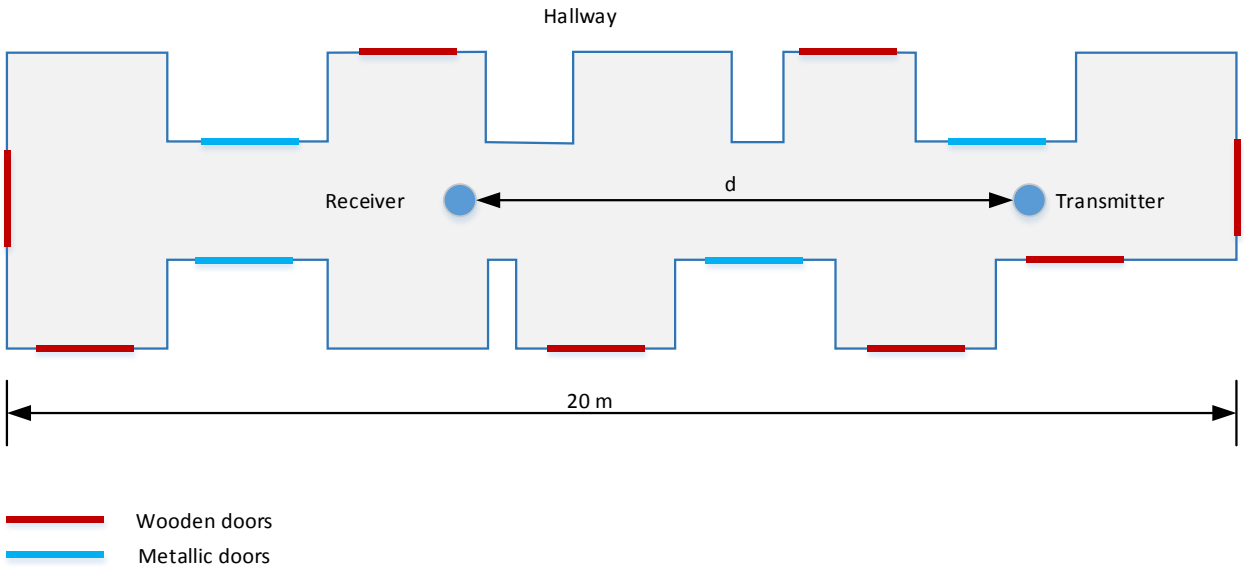

Figure 34: Approximate sketch of the hallway used for performing the range measurements.

To obtain more realistic results, the system was tested indoors in a hallway, i.e. in a rich multipath environment. The sketch of the hallway is given in Figure 34. The walls are made of bricks, reinforced with concrete and metal pillars. Some of the doors are wooden and some of them are metallic, leading to strong reflections. The distance between the stations was changed from 1 to 10 metres, with a step of 40 centimetres. The first set of measurements was performed once more using omnidirectional antennas with 2.5 dBi gain. The obtained distance estimates as a function of the true distance are shown in Figure 35.

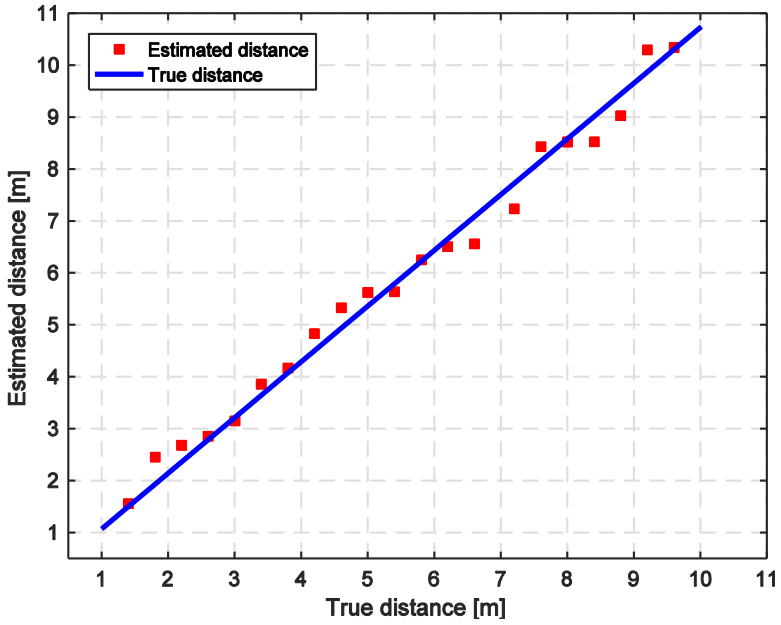

Figure 35: Estimated distance compared to the true distance (hallway; omnidirectional antennas).

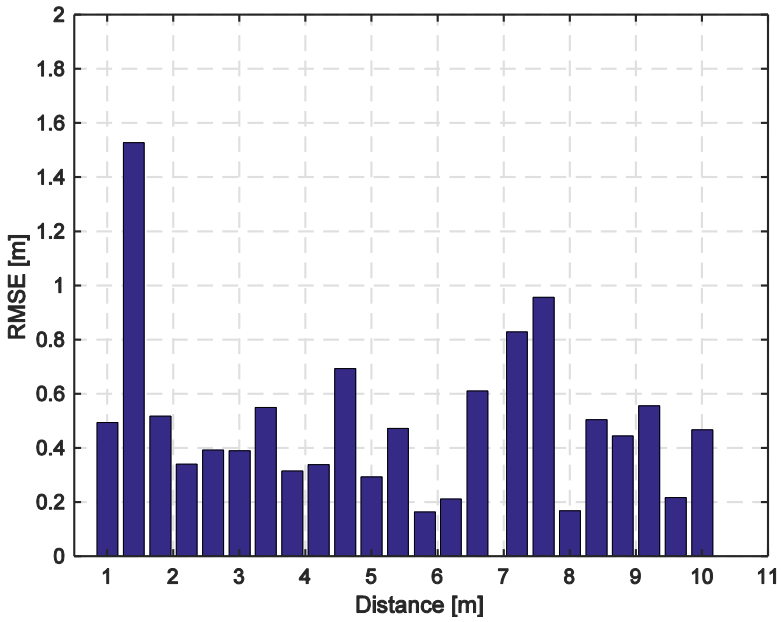

Figure 36: RMSE as a function of distance (hallway; omnidirectional antennas).

The RMSE of the measurements is shown in Figure 36. It can be noticed that the errors are slightly larger compared to the results obtained in the anechoic chamber. The main reason is the large number of reflections from the surrounding walls and metallic doors. In addition, there are people moving around, fact that increases the error in the distance estimation.

The CDF of the measurements carried out in the hallway using omnidirectional antennas is shown in Figure 37. Only a couple of measurements have CDF which are wider compared to the ones obtained in the anechoic chamber. The main reason is that the scenario is not completely static.

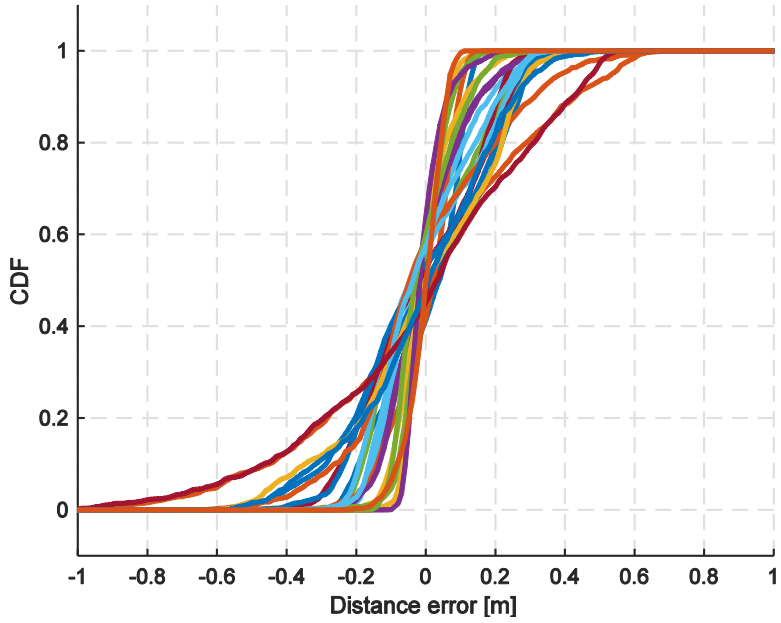

Figure 37: CDF of the estimation error for all of the distances (hallway; omnidirectional antennas).

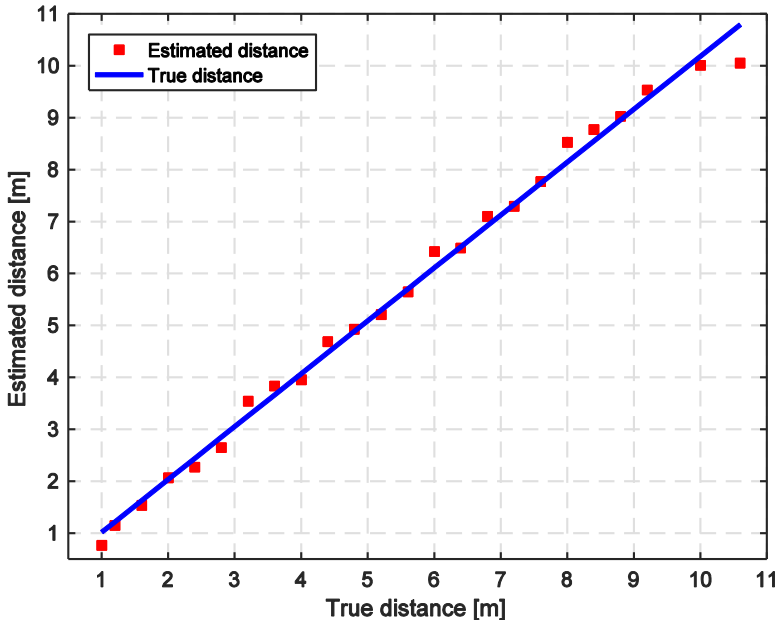

Figure 38: Estimated distance compared to the true distance (hallway; 6 dBi patch antennas).

Finally, we assessed the ranging system in a hallway using 6 dBi gain patch antennas. The larger gain should mitigate the multipath propagation effects, leading to the achievement of better ranging results. In real cases, the small cells would have directional antennas and rarely omnidirectional antennas would be used. In Figure 38 the estimated distances as a function of the true distances are depicted. The estimated distances follow the true distances relatively well. The RMSE is shown in Figure 39. In this case, the RMS distance estimation error is less than 0.8 metres, and is slightly lower compared to the error in the case where omnidirectional antennas are used. The main reason for the lower RMSE is the reduced number of reflections from surrounding objects due to the higher antenna gain.

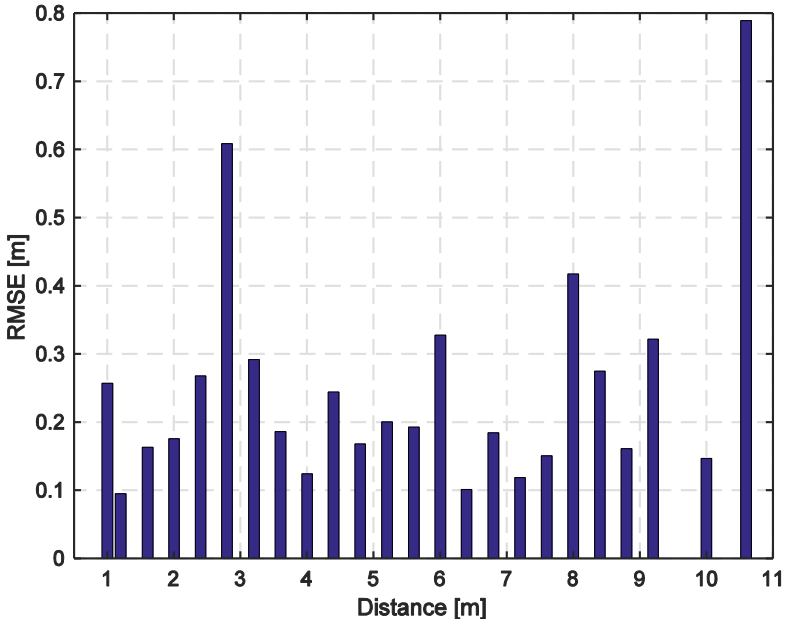

Figure 39: RMSE as a function of distance (hallway; 6 dBi patch antennas).

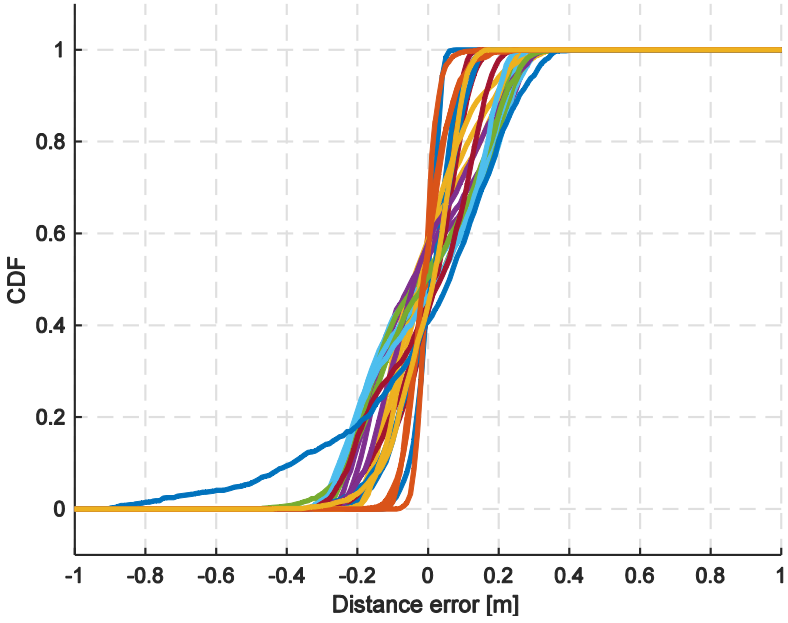

Figure 40: CDF of the estimation error for all of the distances (hallway; patch antennas).

The CDFs obtained for each distance are similar to those obtained in the anechoic chamber, as shown in Figure 40. The transition region is once again the interval of ± 0.3 metres.

From the measurement campaign and associated evaluations, it can be concluded that a ranging precision of less than 1 metre can be achieved in the Sub-6 bands. The ranging precision can be further improved by using advanced distance estimation techniques [61][62][63][64] as well as larger channel bandwidths.

These initial evaluations were performed indoors and they show satisfactory results. Since the main focus in 5G-XHaul is on outdoor scenarios, further evaluations for these scenarios will be performed. Nevertheless, we expect that the ranging and localisation accuracy in outdoor scenarios will outperform that of indoors. Few main factors would contribute to better accuracy. First, higher gain antennas are normally used, which significantly reduces the multipath propagation, in turn improving the localisation accuracy. Second, multipath propagation outdoors is less significant than indoors due to the larger distance the radio signals travel.

4.3 Ranging in the 60 GHz band

There have been many studies on the propagation characteristics of mmWave frequencies (in the 30 to 300 GHz range) [68][69], as well as advances in the design of RF circuits at these frequencies [51][52][53]. On latter topic, 5G-XHaul presented in deliverable D4.9 the initial document on mmWave circuits and systems D4.9 [54]. These studies have demonstrated the feasibility of communication at mmWaves and its ability to support existing and new communication services for mobile users [70].

The higher path loss necessitates the use of narrow and very directional beams. These can be realised through high-gain horn antennas, as well as phased antenna arrays, which can be practically assembled within laptops or smartphones thanks to the order-of-millimetre wavelengths.

In 5G-XHaul we investigate the ranging and localisation precision which can be achieved in the 60 GHz band, which is a candidate for playing a main role in the backhaul (BH) network [3]. The channel bandwidth, according to the IEEE 802.11ad standard considered in 5G-XHaul, is of approx. 2 GHz. The implementation of ranging and localisation algorithms on a 60 GHz platform involves a considerable effort. Due to the large bandwidths and sample rates, the approach adopted for the Sub-6 bands (Section 4.2) is not feasible anymore.

4.3.1 Measurement system description

To investigate the achievable ranging and localisation precision, we setup a system as shown in Figure 41. The measurement setup consists of an arbitrary waveform generator (AWG) Tektronix AWG7122c and a scope LeCroy HDO9404. The signal generated from the AWG is supplied to a 60 GHz analogue front-end (AFE) from Infineon Technologies, which contains the BGT60 chip, also from Infineon Technologies [55]. The main specifications of the AFE are shown in Table 7.

To investigate the ranging precision that can be achieved in the 60 GHz band, one AFE is used as a transmitter and one is used as a receiver. The frequency at which the evaluation was performed is 62.64 GHz. The transmitter is connected to the AWG, who generates the frame to be transmitted. This frame is previously created on a host computer using MATLAB. The second AFE is used as a receiver and is connected to the scope, which digitizes the BB signal acquired at the output of the receiver AFE. The acquired waveform at the scope is saved and is used to estimate of the time-of-arrival (ToA). To further estimate the time-of-flight (ToF) and, therefore, the distance between the transmitter and the receiver, both AWG and scope must be synchronised. This is achieved by using a separate long cable between the two devices. The AWG uses a sample rate of 1 GSps to achieve a signal bandwidth of 500 MHz, and 2 GSps for a signal bandwidth of 1 GHz. These bandwidths are used since the maximum bandwidth supported by the AFE is 1 GHz. The use of higher bandwidths, e.g. 2 GHz, would improve the ranging precision even more. The scope samples at its maximum sample rate of 20 GSps. If the channel bandwidth is 500 MHz, a total of 400000 samples are acquired and, for a channel bandwidth of 1 GHz, a total of 200000 samples are acquired.

The transmitter remains static and the receiver is moved away with respect to it. For each step, around 40 frames are recorded and the ToA is estimated offline on a host computer. The frame format used for this purpose is shown in Figure 42.

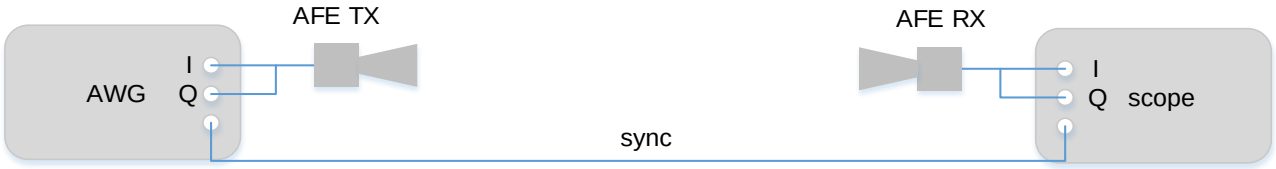

Figure 41: Measurement setup.

Table 7: Main specifications of the Infineon AFE.

Parameter	Value
Name	BGT60
Frequency	57.0 - 64.0 GHz
Output power P_{sat} (typ)	14.0 dBm
Rx Gain (typ)	22.0 dB
Noise figure	7.0 dB
IF Bandwidth (min)	1 GHz

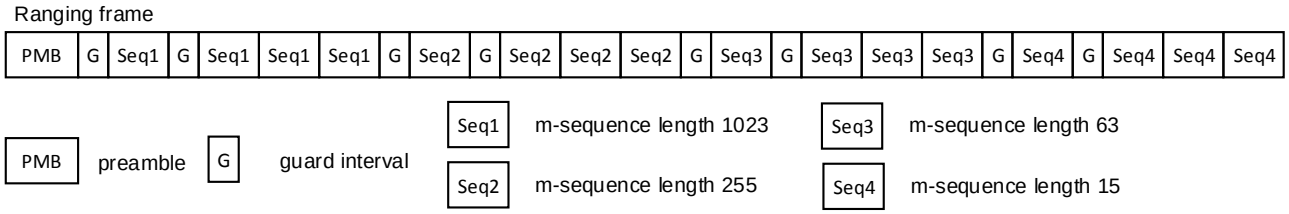

Figure 42: Frame format used for ranging in the 60 GHz band.

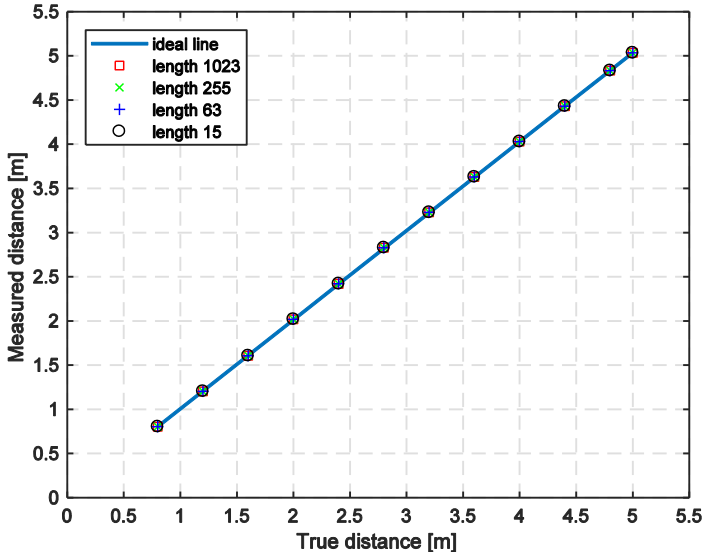

Figure 43: Estimated distance as a function of true distance (anechoic chamber, 500 MHz channel bandwidth, single m-sequence).

The frame consists of a preamble, used for clock offset estimation, and multiple fields containing m-sequences with different lengths used for ToA estimation. The different lengths are used to evaluate the ranging precision as a function of the length of the m-sequence. It can be also noticed that, for each length, there is a single sequence and three concatenated sequences. The main reason for using a single and three concatenated sequences is that the autocorrelation function of a single sequence is different compared to that of a periodic sequence. We cannot use a periodic sequence in this case, but having three concatenated sequence can relatively well represent the periodic case. The ToA estimation is performed using the estimator shown in Figure 18. The ToA of the single m-sequences as well as the ToA of the groups of concatenated m-sequences is estimated.

4.3.2 Measurement campaign

To investigate the distance estimation precision, we carried out two measurement campaigns. The first one was performed in an anechoic chamber, being the second one carried out in a hallway. For both measurement campaigns the measurements were performed for channel bandwidths of 500 MHz and 1 GHz.

Measurements in the anechoic chamber

The anechoic chamber shown in Figure 27 was used for this set of measurements. The two AFEs were initially placed on a distance of 0.8 m. This distance was increased in steps of 40 cm and, for each distance, approximately 40 received frames are acquired. The largest distance for which the ranging precision was evaluated is 5 m due to the space limitations of the anechoic chamber. The transmitter and the receiver are mounted on an electromechanical system, which is electronically controlled and used to change the distance between the AFEs. The AFEs are mounted on a height of 1.2 metres from the ground.

Using the acquired samples, the distance was estimated using either one of the single sequences or using one of the groups of three concatenated sequences. A total of eight distance estimates are obtained using a single received frame. For each distance between the transmitter and the receiver, a total of 16 distance estimates are obtained, since two different channel bandwidths are used.

Figure 43 shows the average distance estimate using 500 MHz channel bandwidth as a function of the true distance. In this figure, only distance estimates obtained using single m-sequence are represented.

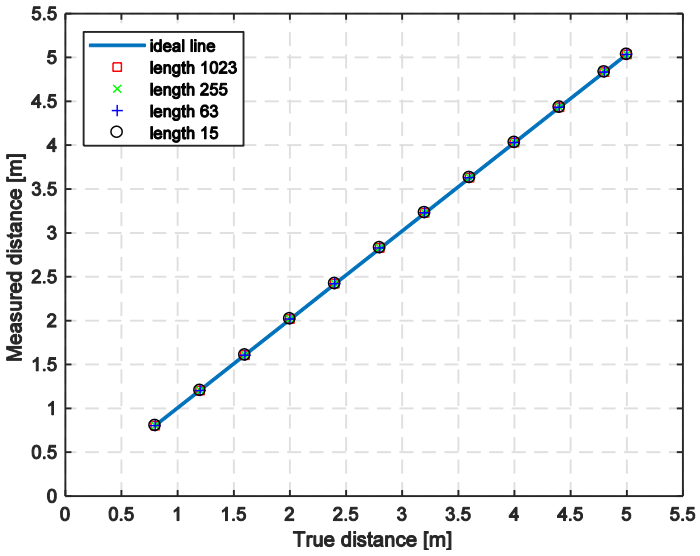

Figure 44: Estimated distance as a function of true distance (anechoic chamber, 500 MHz channel bandwidth, periodic m-sequences).

The deviations of the average value from the true value, as we see in Figure 43, are due to systematic errors introduced by system imperfections as well as due to multipath propagation. It can be noticed that the measurements are fitting almost perfectly to the true distance. This high ranging accuracy is possible due to the large channel bandwidth and the absence of strong reflections in the anechoic chamber.

In Figure 44, the average estimated distance using the three concatenated copies of m-sequences compared to the true distance is plotted. As can be noticed, the deviation from the true distance is also negligible. In both cases (periodic and single m-sequence) the estimated distances are almost the same. This is mainly due to large SNR at the receiver. The SNR for the measurements performed in the anechoic chamber was estimated to be between 21 dB and 28.9 dB. For a channel bandwidth of 1 GHz, the obtained results are the same as the ones shown in Figure 43 and Figure 44 and, therefore, the results are not included.

To further quantify the ranging errors due to noise, the RMSE of the measurements is calculated and shown in Figure 45 for 500 MHz channel bandwidth, and in Figure 46 for 1 GHz bandwidth. As can be noticed, for all of the performed measurements in the anechoic chamber, the RMSE is less than 1 cm in case of 500 MHz and 1 GHz channel bandwidth. The RMSE is relatively constant for all of the distances taken into account since the SNR is relatively high for the measurements performed as stated previously. Lower SNRs were not considered during the evaluation, since this SNR level is needed for higher order modulations like 64QAM, 16QAM, 8PSK, QPSK etc., which are used for high speed wireless data transmissions.

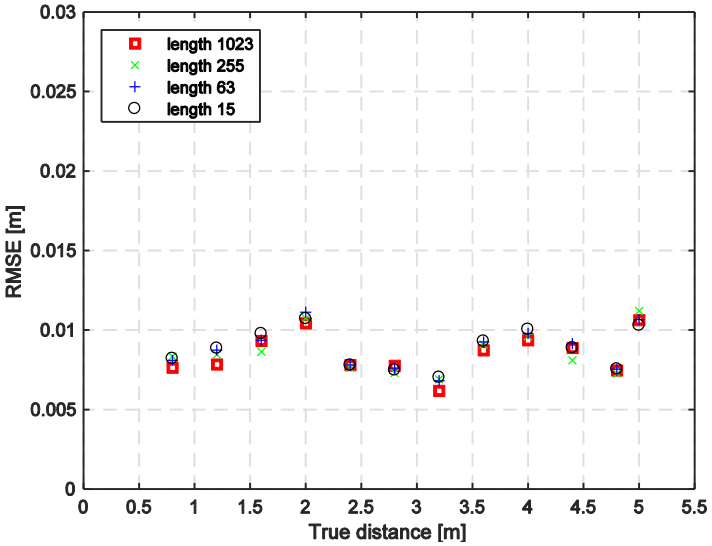

Figure 45: RMSE as a function of distance (anechoic chamber, 500 MHz channel bandwidth, single PN sequence).

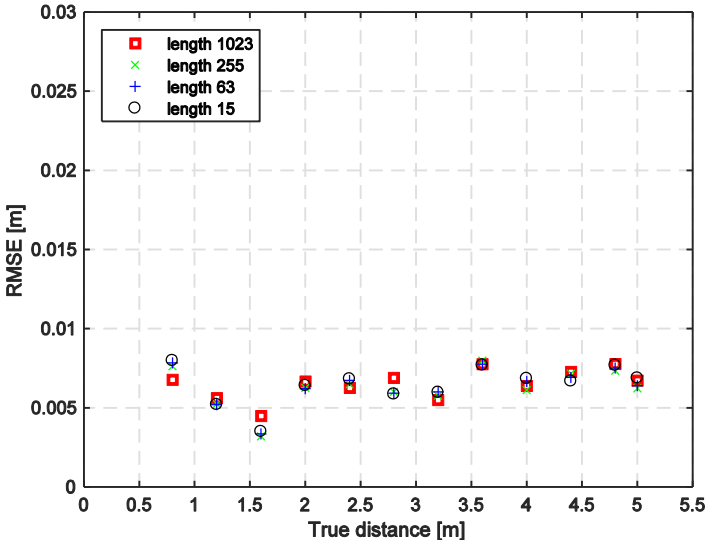

Figure 46: RMSE as a function of distance (anechoic chamber, 1 GHz channel bandwidth, single PN sequence).

The use of periodic m-sequences does not make an improvement to the RMSE and, therefore, additional RMSE plots for the periodic case are not included. Improvements can be only expected in low SNR scenarios.

Figure 47 depicts the CDFs of the ranging errors when considering a single m-sequence of length 1023. As can be noticed, the ranging errors are distributed within the range ± 4 cm. The CDFs for other lengths of the m-sequence and for the periodic case (three concatenated m-sequences) are similar those plotted in Figure 47 and, therefore, they are not included.

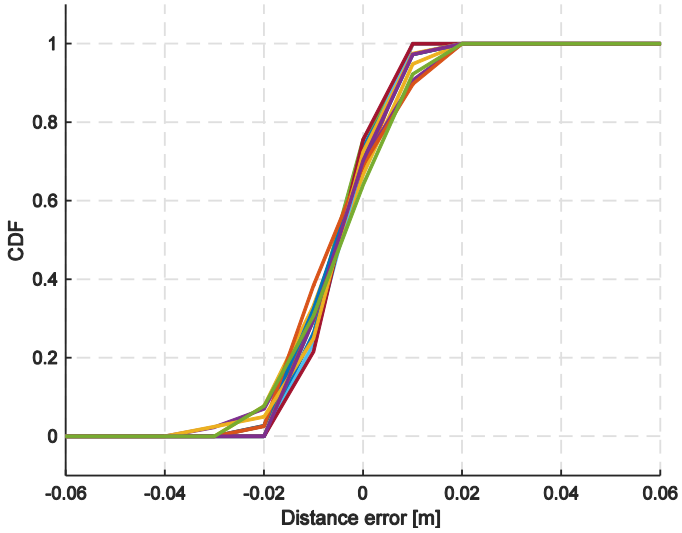

Figure 47: CDF of the distance estimation error with respect to the mean value of the estimates (anechoic chamber, 500 MHz channel bandwidth, PN sequence 1023 bits long).

Measurements in a hallway

The measurements performed in the anechoic chamber were repeated in the hallway represented in Figure 34. The main objective is to evaluate the ranging precision in a more realistic environment. Due to the presence of walls and metallic objects in the hallway, we would expect more reflections which can affect the ranging and, therefore, positioning precision and accuracy. Nevertheless, the use of high gain antennas (20 dBi) mitigates the multipath propagation significantly and, in turn, it would not affect the precision and the accuracy of the distance estimates. The use of high gain antennas is justified since in the commercial systems it is expected that phased arrays with high gain are also going to be used. The measurements performed in the hallway use the same measurement system shown in Figure 41.

For the measurements performed in the hallway, the distance between the transmitter and receiver was increased form 1 meter to 8 meters in steps of 50 centimeters. For each distance, a total of 40 frames were captured and saved. The AFEs are mounted on a movable carts at a height of 80 centimetres. Both I and Q components of the signal are once more captured using two separate channels of the scope. The sync signal is captured using the third channel and is used as a trigger signal for capturing the arriving frame and is also used as a reference, when the ToA is estimated. The estimated SNR of the received signal is in the range of 16.8 – 31 dB.

Samples from the received signal are acquired using the scope and are further processed on a host computer to estimate the ToA. The ToA estimator shown in Figure 18 is used. For each distance, the mean value of the estimated distance is calculated and compared to the true distance. Further the RMSE for each distance is estimated and plotted. Finally, the CDFs of the distance error, with respect to the mean estimated distance is estimated and plotted. The CDFs show the distribution of the ranging error for each distance between the transmitted and the receiver.

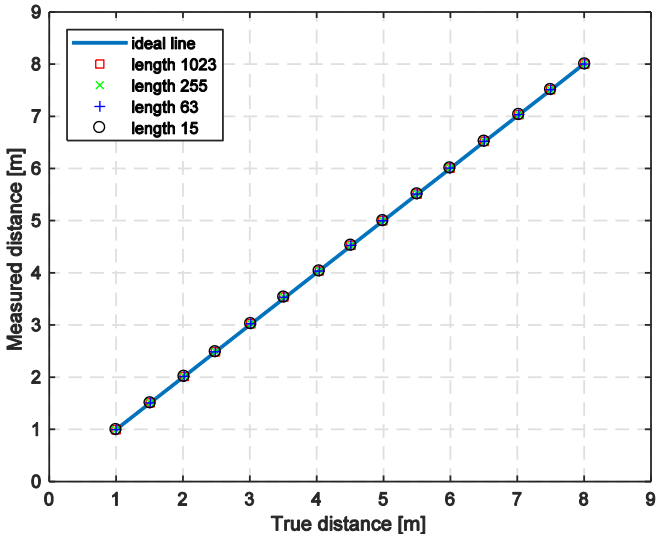

Figure 48: Mean value of the estimated distance as a function of the true distance (hallway, 500 MHz channel bandwidth, single m-sequence).

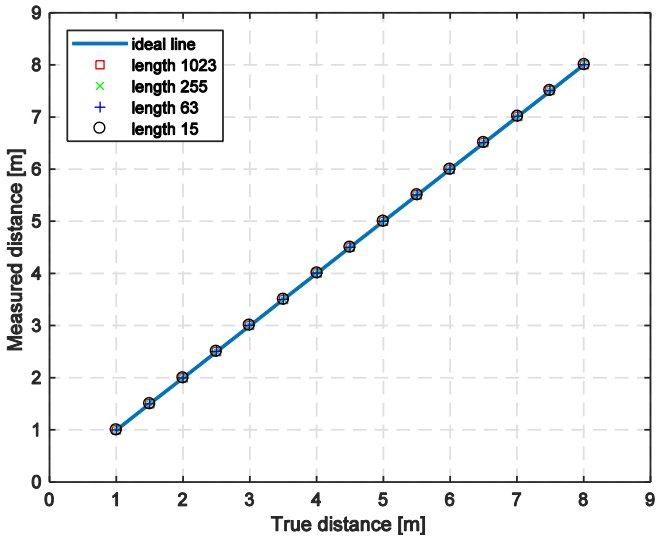

Figure 49: Mean value of the estimated distance as a function of the true distance (hallway, 1 GHz channel bandwidth, single m-sequence).

The measurements in the hallway were performed also using channel bandwidths of 500 MHz and 1 GHz. The mean value of the obtained distance, with respect to the true value is plotted in Figure 48 for channel bandwidth of 500 MHz and in Figure 49 for channel bandwidth of 1 GHz. The mean value of the estimated distance is calculated over the 40 previously estimated distances. It can be noticed that in the both cases the estimated distances follow, almost perfectly, the true distances. The distance estimation errors are small compared to the true distances and cannot be noticed. These are small due to the large signal bandwidth used. Also, due to the high gain antennas the number of the reflections arriving at the receiver is kept at minimum which leads to higher precision of the distance estimation. The relatively high SNR allows high precision distance estimation, even when the length of the m-sequences is small. This is the reason why the distance estimations performed with m-sequences with different lengths are almost the same. The plots of the mean value of the estimated distance in case of periodic m-sequence (three sequential m-sequences) as a function of the true distance, is the same as the plots in Figure 48 and in Figure 49. Therefore, these plots are not included in this deliverable.

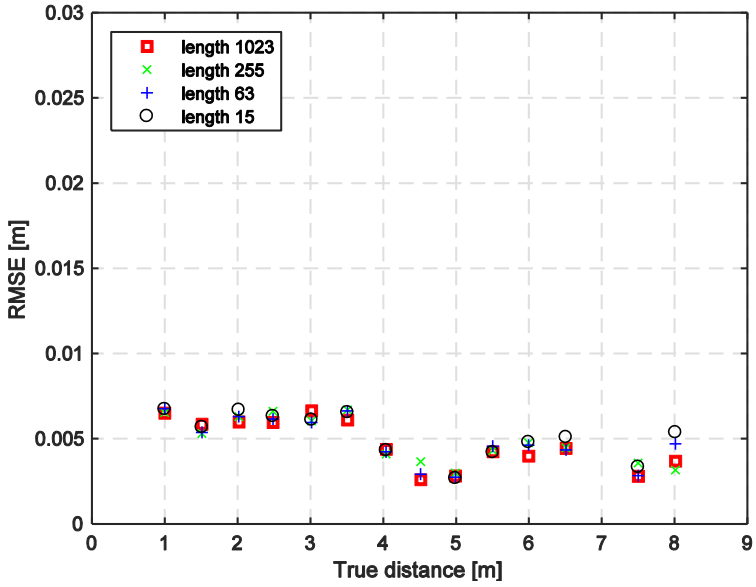

Figure 50: RMSE as a function of distance (hallway, 500 MHz channel bandwidth, single PN sequence).

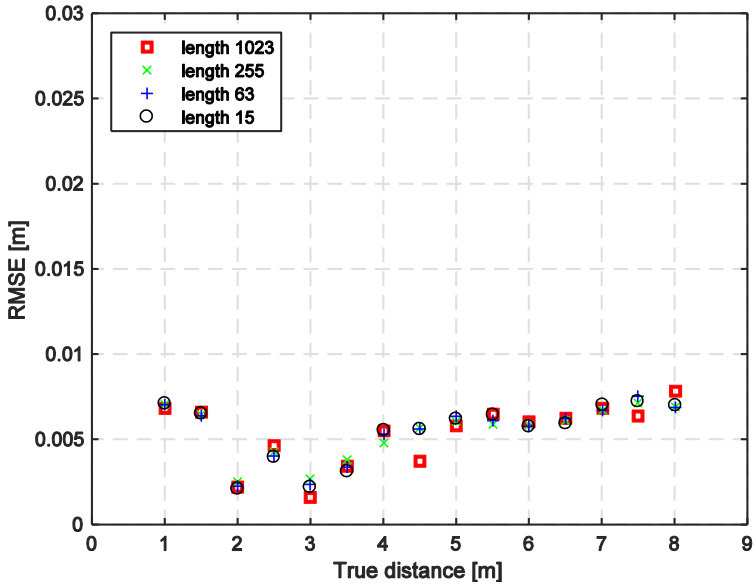

Figure 51: RMSE as a function of distance (hallway, 1 GHz channel bandwidth, single PN sequence).

Using the data from the performed measurements, the RMSE with respect to the true distance is also estimated for each distance between the transmitter and the receiver. The results are shown in Figure 50 for a channel bandwidth of 500 MHz and non-repeating (i.e. non periodic) m-sequence, and in Figure 51 channel bandwidth of 1 GHz. For periodic m-sequences, i.e. when three successive sequences are used, the same plots are obtained and, therefore not shown here. A slight dependency of this error as a function of distance can be noticed in Figure 50 and in Figure 51, and this is a result of the multipath propagation due to the reflections in the hallway. Nevertheless it is not significant due to the high antenna gain and low radiation beam width. It can be noticed that the RMSE in this case is slightly (a couple of millimetres) lower compared to the one in anechoic chamber. This is due to the use of different cables between the AWG, the scope and the AFEs. This can be later compensated, but the main objective was to prove that centimeter precision can be achieved. An error of a few millimeters would not play a significant role.

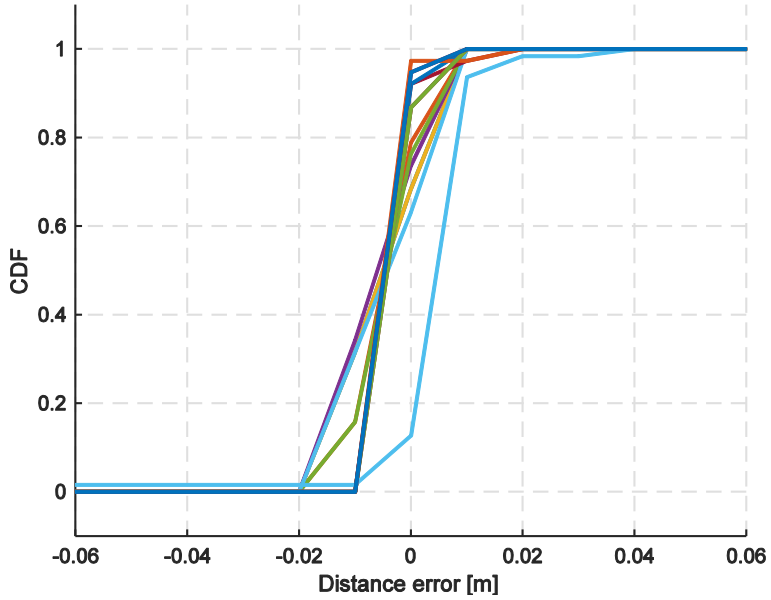

Figure 52: CDF of the measurement error (hallway, 500 MHz channel bandwidth).

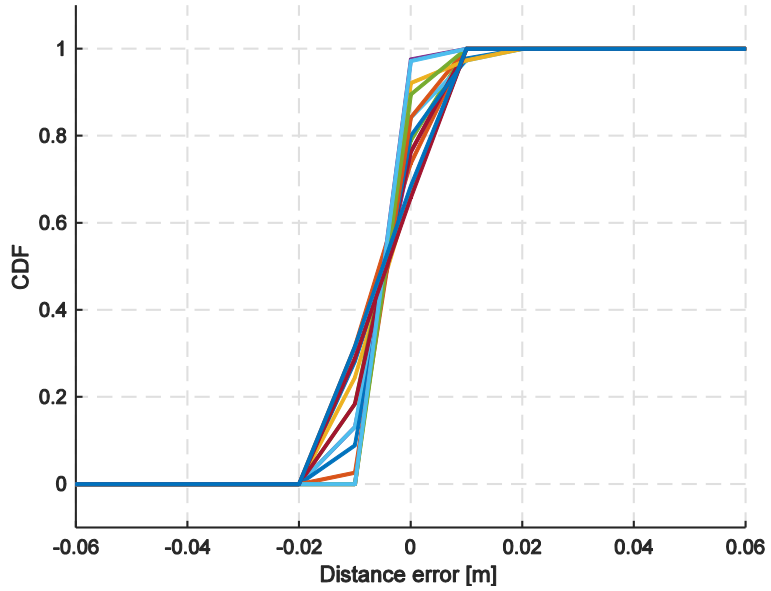

Figure 53: CDF of the measurement error (hallway, 1 GHz channel bandwidth).

Finally, in Figure 52 and Figure 53, the CDF of the distance estimation error is shown. This is the error with respect to the mean value of the estimated distances. These plots consider a single m-sequence measuring different distances, and signal bandwidths of 500 MHz and 1 GHz, respectively. For the remaining lengths of the m-sequences, the plots are almost identical and are not shown. As can be noticed, the distance estimation error for single measurements is not larger than 4 cm.

To summarise, we have used a ToA method to estimate the distance between transmitter and receiver. These were almost perfectly synchronised using a cable. In real scenarios, the synchronisation is not as good as in this case and, therefore, the expected precision would probably be worse. To avoid synchronisation issues TWR is commonly used. In TWR the time of arrival is estimated twice, which would increase the distance estimation error we obtain here. Nevertheless, this error would still remain under 10 cm, which is a satisfactory precision for use in 5G networks.

4.4 Localisation using sequential beacon frames

Localisation, as mentioned in Section 2.2, is usually performed using trilateration. All distances from the anchor nodes to the node with unknown position must be previously estimated and used for position estimation. For 2D position estimation, at least three anchor nodes are needed and, for 3D position estimation, a minimum of four anchor nodes are needed. The required distances can be precisely estimated using TWR. With TWR, a minimum of six frame transmissions would be needed in 2D case, and at least eight frame transmissions in the 3D case for each node whose position should be estimated. This applies in case the negotiation for ranging and positioning is performed using frames for data transmission which carry the additional data for localisation. If the negotiation is performed using separate data frames, the number of frames transmitted for position estimation of a single node can become significantly higher. In dense and mobile scenarios, where the number of stations is high, and whose positions must be estimated frequently, the use of the wireless medium for localisation purposes can become significant.

To solve the mentioned issues with the high number of frames transmission needed for position estimation, in 5G-XHaul we propose a method which can be used for joint localisation of large number of mobile stations (UEs), without increasing the number of needed transmissions [65][66]. The proposed method is presented in the time diagram in Figure 54.

To carry out position estimation of multiple mobile stations using the same transmitted frames, the UEs must be able to receive the frames transmitted from different anchor nodes. The mobile stations do not perform any transmission. In case beam steering is used, the beams must be wide enough to cover multiple mobile stations.

4.4.1 System and method description

The system consists of four anchor stations, e.g. small cells, labelled as ***A₁***, ***A₂***, ***A₃*** and ***A₄***, and two mobile stations labelled as ***M₁*** and ***M₂***. The position of the anchor stations is known and the position of the mobile stations should be estimated. It is assumed that both mobile stations are able to receive the frames from the four anchor stations.

The localisation procedure starts from station ***A₁*** at time T_1. The station ***A₁*** synchronizes with station ***A₂*** and transmits a localisation frame, loc_1, to mobile stations ***M₁*** and ***M₂***. Then, station ***A₂*** synchronizes with station ***A₃*** at time T_2 and transmits a broadcast frame to mobile nodes ***M₁*** and ***M₂***. The same process is performed by node ***A₃*** and, finally, node ***A₄*** only transmits a broadcast frame to the mobile nodes ***M₁*** and ***M₂***. These frames are usually referred to as beacon frames. They are transmitted in a sequential manner, in order to avoid and/or minimize position estimation errors due to clock frequency inaccuracy and clock frequency offset between the anchor nodes.

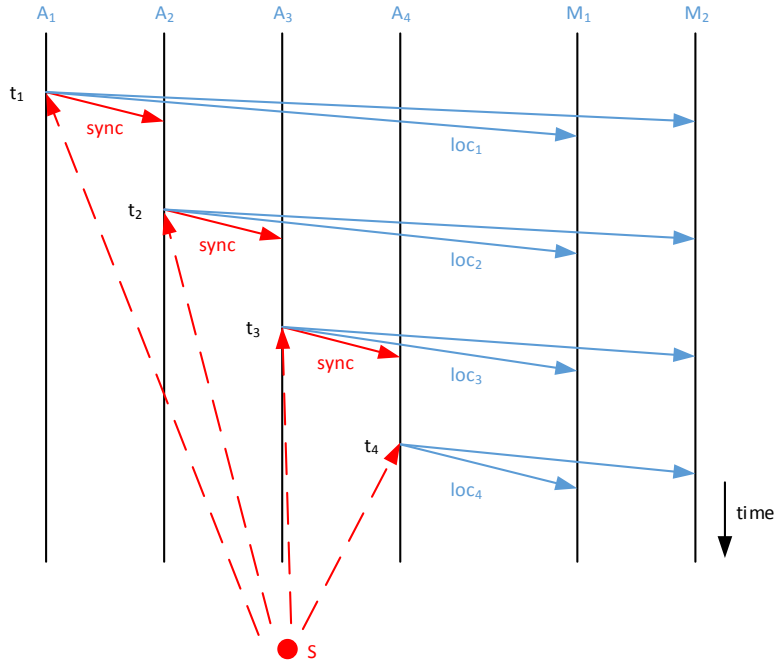

Figure 54: Time diagram of the proposed localisation method.

Synchronisation is extremely important in the proposed method, and can be achieved using different approaches. The **first approach** involves using the localisation frames loc_1, loc_2, loc_3 and loc_4, also for synchronisation of the anchor stations. In this approach, the anchor stations must be able to receive the broadcast frames, which is not always possible. The **second approach** is to use separate frames for synchronisation between the anchor stations. These frames can be transmitted wirelessly or by using wires, at the same time or nearly at the same time when the localisation frames are transmitted. For example, the synchronisation between all of the anchor stations can be performed and immediately the localisation frames can be transmitted. Finally, the last approach is to use a separate entity which synchronizes all of the anchor stations. This entity is labelled as *S* in Figure 54. It is important to transmit the localisation frames as soon as the synchronisation is performed, since the clocks of the anchor stations would drift due to the existing clock frequency offset and, therefore, would affect the precision of the estimated position. By keeping the interval between the synchronisation and transmission of the localisation frames small, the distance estimation error would also be small.

The localisation frames loc_1, loc_2, loc_3 and loc_4 are transmitted at time t_1, t_2, t_3 and t_4 respectively. These times are previously negotiated and are measured with the same time reference since the anchor stations are synchronised in advance. The time intervals between the transmissions would be also known. Nevertheless, the intervals between the reception of the localisation frames at mobile stations $\boldsymbol{M_1}$ and $\boldsymbol{M_2}$ are not going to be the same to the intervals between the transmitted localisation frames. This is due to the time-of-flight (ToF) needed for the frames to travel from the anchor stations to the mobile stations. The intervals between the receptions of the localisation frames at the mobile stations would be different if the positions of the mobile stations are different.

The mobile stations can estimate their position by simply measuring the intervals between the receptions of the localisation frames. This method is basically a time-of-arrival method. The mobile stations estimate the time of arrival of each localisation frame and estimate its own position. Basically, for a 2D localisation, a total of three anchor stations are needed. Nevertheless, if the mobile stations are not synchronised to the anchor station a total of four anchor stations would be needed for 2D localisation. The four anchor stations are needed since the absolute time at which the localisation frames were transmitted is not known at the mobile stations. For 3D localisation a total of five anchor stations are required. The details about position estimation in a ToA scenario can be found in [71].

The transmissions of the anchor stations can be used for position estimation by unlimited number of mobile stations. Nevertheless, all of the mobile stations must receive the same broadcast frames. In the Sub-6 bands this is usually not an issue since the beam widths are wide and multiple stations can receive the same transmitted signals. In mmWave bands, the beam widths are narrower and this method is hardly applicable to multiple stations.

4.4.2 Extension of the proposed method

Using the method described before, the position is estimated at the mobile station. The mobile station can transmit its position to the network, but in some scenarios it is also important for the network to be able to estimate the position of the mobile station. Therefore, we further extend this method as shown in the time diagram in Figure 55. The anchor stations synchronise and transmit the localisation frames. The mobile stations can estimate their positions using these localisation frames. Further, some of the mobile stations can transmit a frame which would be received by the anchor stations. This frame would be received at the anchor stations in different time instants due to the different distances and, therefore, different ToFs between the mobile station and the anchor stations. The time of arrival of the frame in each station is measured with respect to a local clock in each of the anchor stations. These clocks are synchronised just before the localisation took place, which guaranties that the clocks in different anchor stations have not significantly drifted. Having the time-of-arrival of this frame at each anchor station, the position of the mobile stations can be easily estimated. In order to estimate the position of the mobile station, all the estimated ToAs are needed. The anchor nodes can supply these ToAs to the localisation server which would estimate the position of the mobile station.

The position of the mobile station in this case can be also estimated using TWR, instead of using the ToA at the anchor stations. As shown in Figure 55, a TWR scenario is performed between each of the anchor stations $\boldsymbol{A_1}$, $\boldsymbol{A_2}$, $\boldsymbol{A_3}$ and $\boldsymbol{A_4}$, and the mobile station $\boldsymbol{M_1}$. In this case the network can estimate only the position of the mobile station $\boldsymbol{M_1}$. The TWR between the anchor station $\boldsymbol{A_1}$ and the mobile station $\boldsymbol{M_1}$ is performed using the frames loc_1 and $repl_1$. The TWR between $\boldsymbol{A_2}$ and $\boldsymbol{M_1}$ is performed using the frames loc_2 and $repl_1$. The same applies for the TWR between the nodes $\boldsymbol{A_3}$, $\boldsymbol{A_4}$ and $\boldsymbol{M_1}$. Using the TWR between the mobile station and each of the anchor stations, the distance between them can be estimated. The position can be further estimated

using trilateration. The advantage of estimating the position using TWR is that the anchor nodes must not be perfectly synchronised in order to precisely estimate the position of the mobile station.

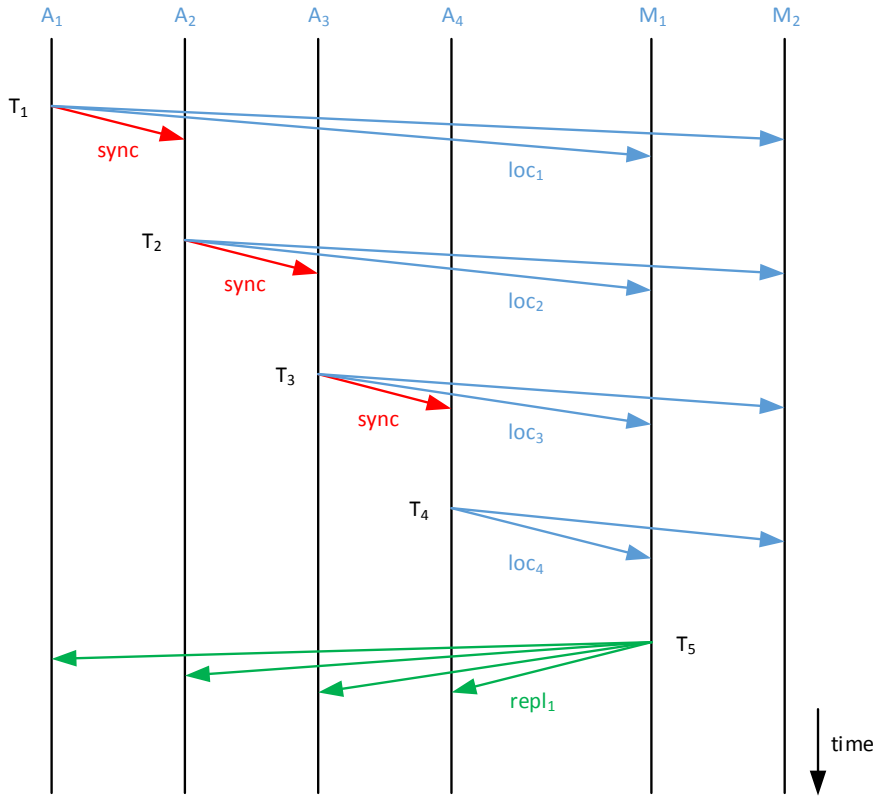

Figure 55: Extended version of the proposed localisation method.

The proposed method can be easily implemented in the small cells and be used for location estimation of UEs. The synchronisation precision previously discussed in the synchronisation section is significantly good for performing the TWR. The main advantage is that the number of transmissions is significantly lower compared to a TWR performed between each small cell and UE. In this case, each small cell should perform for example one transmission and each UE should perform one transmission. Keeping the number of transmissions low is extremely important in dense and dynamic scenarios.

It is expected that in the future localisation methods which reduce the number of transmissions are going to be favoured. This is of special interest in dense RANs, where due to the large number of users, the number of required transmissions is significant.

5 Interoperability of 5G-XHaul wireless technologies

In the 5G-XHaul wireless architecture, small cells can be wirelessly backhauled to macro-cell sites using a combination of mmWave and Sub-6 wireless technologies [3]. This can result, for urban deployments, in an ideal combination of capacity and coverage.

Both mmWave and Sub-6 nodes can act both as TNs and ANs, respectively, and are even expected to be co-located in some scenarios. This represent an interesting benefit from a flexibility perspective since the techniques presented so far in this deliverable can be either used or shared for both transport network as well as in the RAN.

The co-location of the nodes can, on one hand, reduce the complexity and communication exchange among nodes since the available synchronisation signal could be used for both interfaces, which, as a result, will mitigate contention and interference thus improving performance. On the other hand, another benefit would be the use of Sub-6 technologies for coarse localisation (given the limitations stated in previous sections), being mmWave localisation the choice for a fine precision estimation of the position of the nodes (users). It is expected that not always high accuracy is desirable, e.g. when the mobility of the users UE's is estimated.

5.1 Shared synchronisation of co-located Sub-6 and mmWave nodes

As stated before, co-located Sub-6 GHz and mmWave nodes should avoid redundant synchronisation mechanisms in order to reduce the amount of signalling, and to save energy. When a low latency wired connection is available at the node location, standard synchronisation mechanisms (cf. Section 2.1.2) must be carried out through that interface (as it was the case in the experiments reported in deliverable D4.11 [72]). Otherwise, synchronisation using mmWave links should be prioritised over Sub-6 GHz when possible, due to the higher reliability and predictability of the medium access in those bands.

Exceptions to these rules, however, should be contemplated in some situations. For example, in cases where, despite the possibility of receiving synchronisation from a mmWave interface, there is a downlink neighbouring TN that can only be reached by means of the Sub-6 GHz interface. In such case, the TN must behave either as a transparent clock, or as a master to that downlink neighbour.

5.2 Shared localisation between Sub-6 and mmWave nodes

As stated in deliverable D2.2 [3], the 5G-XHaul Sub-6 nodes (either acting as TNs or ANs) could be used for discovery of surrounding TNs or RAN elements (UEs) more easily thanks to wide beam antennae (omnidirectional, in some cases), and the possibility of NLoS communication. On one hand, this favours TN discovery in the transport network. For example, Sub-6 could assist in the creation of mmWave BH links on the discovery of other TNs in the range. On the other hand, as we presented in deliverable D3.1 [73], information about the status of the RAN should be available for the transport network control since the dynamicity of UEs impact the transport network. In a dense urban environment, UEs will have multiple network attachment possibilities, which will change in time as the user moves. The information gathered will enable the transport network to more effectively balance the traffic load between base stations and mobile network functions across different paths. This can result in a better utilsation of resources within the transport, as well as in an overall improvement of the Quality of Experience (QoE).

Sub-6 technologies can then provide coarse position and/or direction estimate of the UE location using the techniques described in this deliverable, for then having (if required) a finer estimation of the position of the user by performing location estimation in mmWave. The mmWave interface can then be used to establish a high data rate communication with the RAN point of attachment if required.

More information will be included in 5G-XHaul deliverables D3.2 and D3.3, where we will leverage from the localisation techniques presented in this deliverable, to estimate the UEs' position in the RAN.

6 Conclusions and final remarks

In this deliverable we provide the synchronisation methods and techniques to be adopted in the 5G-XHaul wireless data plane, which was already introduced in deliverable D2.2. Based on the current state-of-the-art and the previous experience of the partners involved in the wireless part of the project, we enumerate and describe the different techniques accounting on what is required in 5G.

Regarding synchronisation, this deliverable describes the existing synchronisation technologies, and provides a deeper view of how these techniques may be used to provide frequency and phase synchronisation. The envisioned requirements associated 5G network architectures are addressed, and the challenges of providing clocks to small cells when the BH uses mmWave using the standards 802.11ad/ay have been studied.

With respect to localisation and ranging, the 5G-XHaul project and, in turn, this deliverable, investigates ranging methods that can be used for positioning using trilateration. Regarding technologies, we refer to the two that are currently under study in 5G-XHaul, namely Sub-6 and mmWave at 60 GHz. Concretely, in this first development step, we present experiments carried out in both frequency bands, assessing the algorithms using measurement systems in different indoor scenarios. It is planned to run these algorithms in outdoor scenarios to confirm these promising results, where we expect a reduced influence of multipath propagation given the limited number of reflections. The localisation algorithm proposed in Section 4.4 is also planned to be implemented and evaluated on a SDR platform. Indoor and outdoor tests would be performed in order to determine the positioning accuracy that can be obtained in a real scenario using the TWR methods as well as the proposed localisation method which utilises sequential beacons.

To summarize, this deliverable has illustrated the different synchronisation and localisation methods to be used in the course of the project duration. These methods, in later stages, will be evaluated and demonstrated in realistic scenarios. The upcoming results in these topics will be included in both WP3 and WP5- related deliverables.

7 References

[1] D. Bladsjo, et.al., "Synchronisation aspects in LTE Small Cells," IEEE Comm. Mag., vol.51, no.9, pp.70,77, Sep. 2013.

[2] 5G-XHaul, Deliverable D2.1 – "Requirements Specifications and KPIs Document", November 2015, [Online]. Available: http://www.5g-xhaul-project.eu/download/5G-XHaul_D_21.pdf, Accessed 20 Feb. 2017.

[3] 5G-XHaul, Deliverable D2.2 – "System Architecture Definition", July 2016, [Online]. Available: http://www.5g-xhaul-project.eu/download/5G-XHaul_D_22.pdf. Accessed Feb. 20, 2017.

[4] X. Ge et al., "5G ultra-dense cellular networks," IEEE Wireless Commun., vol. 23, no. 1, pp. 1_15, Feb. 2016.

[5] G. Han, J. Jiang, C. Zhang, T. Q. Duong, M. Guizani, and G. K. Karagiannidis, "A survey on mobile anchors assisted localisation in wireless sensor networks",' IEEE Commun. Surveys Tutorials., vol. 18, no. 3, pp. 2220_2243, 3rd Quart., 2016.

[6] 5G-PPP brochure MWC – https://bscw.5g-ppp.eu/sec/bscw.cgi/d145591/5GPPP-brochure-MWC17.pdf

[7] J. Schiller and A. Voisard, Location-based services. Elsevier, 2004.

[8] 3GPP, "Location Services (LCS); broadcast network assistance for Enhanced Observed Time difference (E-OTD) and Global Positioning System (GPS) positioning methods," 3rd Generation Partnership Project (3GPP) TS 04.35, 2002, http://www.3gpp.org/ftp/Specs/html-info/0435.htm.

[9] C. Y. Chen; W. R. Wu, "3D Positioning for LTE Systems," in IEEE Transactions on Vehicular Technology , vol.PP, no.99, pp.1-1

[10] I. Bisio, F. Lavagetto, M. Marchese and A. Sciarrone, "Energy efficient WiFi-based fingerprinting for indoor positioning with smartphones," 2013 IEEE Global Communications Conference (GLOBECOM), Atlanta, GA, 2013, pp. 4639-4643.

[11] "Timing characteristics of synchrononous Ethernet equipment slave clock (EEC)", ITU-T, ITU-T G.8262/Y.1362, August 2013.

[12] "Timing and synchronisation of LTE-TDD and LTE-Advanced Mobile Networks", Symmetricom, White Paper.

[13] "Standard for Information Technology Telecommunications and Information Exchange between systems. Part 11: Wireless LAN – MAC and PHY Specifications. Amendment 3 : Enhancement for Very High Throughput in the 60 GHz band"; IEEE 28 December 2012.

[14] IEEE P802.11 - Task Group ay, http://www.ieee802.org/11/Reports/tgay_update.htm

[15] "Timing and synchronisation aspects in packet networks", ITU-T, ITU-T G.8261/Y.1361, August 2013.

[16] "Distribution of timing information through packet networks", ITU-T, ITU-T G.8264/Y.1364, May 2014.

[17] "1588-2008 - IEEE Standard for a Precision Clock Synchronisation Protocol for Networked Measurement and Control Systems", IEEE 2008.

[18] "Precision time protocol telecom profile for phase/time synchronisation with full timing support from the network", ITU-T, ITU-T G.8275.1/ Y.1369.1, June 2016.

[19] "Precision time protocol telecom profile for phase/time synchronisation with partial timing support from the network", ITU-T, ITU-T G.8275.2/ Y.1369.2, June 2016.

[20] "On improving clock synchronisation accuracy for LTE-A networks", V.D. Philip & A. Kaoru, VTC-Fall 2015.

[21] "Synchronous Ethernet: A Method to Transport Synchronisation ", Ferrant J. et al., IEEE Communications Magazine, September 2008, pp. 126-134.

[22] "NGFI, The xHaul2, I. Chih-Lin et al., Globecom Workshop 2015.

[23] "Base Station (BS) radio transmission and reception (Release 14)", 3GPP TS36.104, Version 14.1.0, September 2016.

[24] NGMN Alliance, "5G white paper," Mar. 2015. [Online]. Available: http://www.ngmn.org/5g-white-paper.html

[25] 5G Forum, "5G white paper: New wave towards future societies in the 2020s," Mar. 2015. [Online]. Available: http://www.5gforum.org/5GWhitePaper/5G Forum White Paper Service.pdf

[26] A. Mahmood, G. Gaderer, H. Trsek, S. Schwalowsky and N. Kerö, "Towards high accuracy in IEEE 802.11 based clock synchronisation using PTP," 2011 IEEE International Symposium on Precision Clock Synchronisation for Measurement, Control and Communication, Munich, 2011, pp. 13-18.

[27] 5G-PPP, "5G empowering vertical industries, "Feb. 2015. [Online]. Available: https://5g-ppp.eu/wp-content/uploads/2016/02/BROCHURE 5PPP BAT2 PL.pdf
[28] "SyncE and IEEE 1588: Sync Distribution for a Unified Network", Silicon Labs, White Paper
[29] "Packet over Transport aspects – Synchronisation, quality and availability target", ITU-T G.8264/Y.1364, May 2014.
[30] Fang, B. T. (1986). Trilateration and extension to Global Positioning System navigation, Journal of Guidance Control Dynamics, 9:715–717.
[31] Karl, H. and Willig, A. (2005). Protocols and Architectures for Wireless Sensor Networks. John Wiley & Sons.
[32] Rappaport, T. S. et al. (1996). "Wireless communications: principles and practice," volume 2. Prentice Hall PTR New Jersey.
[33] Murphy Jr., W. S. and Hereman, W. (1995). Determination of a Position in Three Dimensions using Trilateration and Approximate Distances. Technical Report, MCS-95-07.
[34] Patwari, N., Ash, J. N., Kyperountas, S., Hero, A. O., Moses, R. L., and Correal, N. S. (2005). Locating the nodes: cooperative localisation in wireless sensor networks. IEEE Signal Processing Magazine, 22(4):54–69.
[35] Green, M. P. (2005). N-Way Time Transfer ("NWTT") Method for Cooperative Ranging. Contribution 802.15-05-0482-00-004a to the IEEE 802.15.4a Ranging Subcomittee.
[36] Bisio, I., Lavagetto, F., Marchese, M., and Sciarrone, A. (2013). Energy efficient WiFibased fingerprinting for indoor positioning with smartphones. In 2013 IEEE Global Communications Conference (GLOBECOM), pages 4639–4643.
[37] Friis, H. T. (1946). A Note on a Simple Transmission Formula. Proceedings of the IRE,34(5):254–256.
[38] Patwari, N. (2005). Location estimation in sensor networks. PhD thesis, Citeseer.
[39] Galov, A., Moschevikin, A., and Voronov, R. (2011). Combination of RSS localisation and ToF ranging for increasing positioning accuracy indoors. In 2011 11th International Conference on ITS Telecommunications, pages 299–304.
[40] Kaplan, E. (1996). Understanding GPS: Principles and Applications. Artech House telecommunications library. Artech House.
[41] Ehrig, M., Petri, M., Sark, V., Gutierrez Teran, J., and Grass, E. (2014). Combined high-resolution ranging and high data rate wireless communication system in the 60 GHz band. In Positioning, Navigation and Communication (WPNC), 2014 11th Workshop on, pages 1–6.
[42] Liu, X., Zhang, H., Gulliver, T. A., and w. Xu, L. (2015). Ranging performance with 60 GHz signals in indoor residential environments. In 2015 IEEE Pacific Rim Conference on Communications, Computers and Signal Processing (PACRIM), pages 70–73.
[43] T. Manabe, Y. Miura, and T. Ihara, "Effects of antenna directivity on indoor multipath propagation characteristics at 60 GHz," in Proc. 6th IEEE Int. Symp. Pers. Indoor Mobile Radio Commun. (PIMRC)/Wireless Merging Inf. Superhighway, vol. 3, Sep. 1995, pp. 1035–1039.
[44] S. Kutty and D. Sen, "Beamforming for Millimeter Wave Communications: An Inclusive Survey," in IEEE Communications Surveys & Tutorials, vol. 18, no. 2, pp. 949-973, Secondquarter 2016.
[45] Lanzisera, S. and Pister, K. (2008). Burst Mode Two-Way Ranging with Cramer-RaoBound Noise Performance. In Global Telecommunications Conference, 2008. IEEE GLOBECOM 2008. IEEE, pages 1–5.
[46] Liu, N. (2010). Performance of Time Delay Estimation and Range-Based Localization in Wireless Channels. PhD thesis, UC Riverside.
[47] Ohlemueller, T., Winkler, F., and Grass, E. (2010). Radio localisation in OFDM networks using the round trip phase. In Positioning Navigation and Communication (WPNC), 2010 7th Workshop on, pages 23–27.
[48] Ettus Research, www.ettus.com
[49] Farnett, E. C. and Stevens, G. H. (1990). Pulse compression radar. Radar handbook, 2:10–1
[50] IEEE Standard for Telecommunications and Information Exchange Between Systems - LAN/MAN Specific Requirements - Part 11: Wireless Medium Access Control (MAC) and physical layer (PHY) specifications: High Speed Physical Layer in the 5 GHz band. IEEE Std 802.11a-1999, pages 1–102.
[51] A. Valdes-Garcia et al., "A Fully Integrated 16-Element Phased-Array Transmitter in SiGe BiCMOS for 60-GHz Communications," in IEEE Journal of Solid-State Circuits, vol. 45, no. 12, pp. 2757-2773, Dec. 2010.

[52] M. Elkhouli et al., A 60 GHz eight-element phased-array receiver front-end in 0.25 mm SiGe BiCMOS Technology, International Journal of Microwave and Wireless Technologies, 2012.
[53] S. Glisic et al., “Fully-Integrated 60 GHz Transceiver in SiGe BiCMOS, RF Modules, and 3.6 Gbit/s OFDM Data Transmission,” in International Journal of Microwave and Wireless Technologies, 3(2), pp. 139–145, Mar. 2011.
[54] 5G-XHaul deliverable D4.9 – Initial report on mm-Wave circuits and systems for high rate point to multipoint links, Available: http://www.5g-xhaul-project.eu/download/5G-XHaul_D_21.pdf, Accessed 31 Mar. 2017.
[55] Infineon BGT60, http://www.infineon.com/cms/en/product/
[56] 5G-PPP “5G Vision”, Feb. 2015, https://5g-ppp.eu/wp-content/uploads/2015/02/5G-Vision-Brochure-v1.pdf
[57] S. Singh et al., “Interference analysis for highly directional 60 GHz mesh networks,” IEEE/ACM TON, vol. 19, no. 5, pp. 1513-1527, 2011.
[58] F. Lemic et al.,”Experimental Evaluation of RF-based Indoor Localisation Algorithms Under RF Interference,” in ICL-GNSS’15, 2015.
[59] S. Sur et al. “60 GHz indoor networking through flexible beams: a link-level profiling,“ 2015.
[60] H. Wang et al., “A survey of range-based localisation algorithms for cognitive radio networks,” in CECNet’12, IEEE, 2012, pp. 844-847.
[61] Humphrey, D. and Hedley, M. (2008). Super-Resolution Time of Arrival for Indoor Localization. In 2008 IEEE International Conference on Communications, pages 3286–3290.
[62] Humphrey, D. and Hedley, M. (2009). Prior Models for Indoor Super-Resolution Time of Arrival Estimation. In VTC Spring 2009 - IEEE 69th Vehicular Technology Conference, pages 1–5.
[63] Jing, L., Liang, P., Maoyong, C., and Nongliang, S. (2008). Super-resolution time of arrival estima-tion for indoor geolocation based on IEEE 802.11 a/g. In 2008 7th World Congress on Intelligent Control and Automation, pages 6612–6615.
[64] Li, X. and Pahlavan, K. (2004). Super-resolution TOA estimation with diversity for indoor geoloca-tion. IEEE Transactions on Wireless Communications, 3(1):224–234.
[65] Efficient Positioning Method Applicable in Dense Multi User Scenarios IEEE 802.11 WLAN WORKING GROUP SESSIONS (Interim), Warsaw, September 12 - 16, 2016, Poland.
[66] Precise Positioning Using Time of Arrival with Pseudo-Synchronized Anchor Nodes IHP.463. DE-Patentanmeldung am 08.12.2016, AZ: DE 10 2016 123 794.9.
[67] ETSI, EN. "300 328 V1. 8.1 (2012-04)." Electromagnetic compatibility and Radio spectrum Matters (ERM); Wideband transmission systems; Data transmission equipment operating in the 2, 4 GHz ISM band and using wide band modulation techniques; Harmonized EN covering essential requirements un-der article 3.2 of the R&TTE Directive (2012).
[68] S. Rangan, T. Rappaport, and E. Erkip, “Millimeter-wave cellular wireless networks: Potentials and challenges,” Proceedings of the IEEE, vol. 102, no. 3, pp. 366–385, Mar. 2014.
[69] T. S. Rappaport, G. R. MacCartney, M. K. Samimi and S. Sun, "Wideband Millimeter-Wave Propagation Measurements and Channel Models for Future Wireless Communication System Design," in IEEE Transactions on Communications, vol. 63, no. 9, pp. 3029-3056, Sept. 2015.
[70] A. Osseiran et al., “Scenarios for 5G mobile and wireless communications: the vision of the METIS project,” IEEE Commun. Mag., vol. 52, no. 5, pp. 26–35, May 2014.
[71] Tsui, James Bao-Yen. Fundamentals of global positioning system receivers: a software approach. Vol. 173. John Wiley & Sons, 2005.
[72] 5G-XHaul deliverable D4.11, “Wireless backhauling using Sub-6 GHz systems”, (draft, pending review by the EU).
[73] 5G-XHaul Project - Deliverable 3.1, “Analysis of state of the art on scalable control plane design and techniques for user mobility awareness. Definition of 5G-XHaul control plane requirements,” 15 July 2016. [Online]. Available: http://www.5g-xhaul-project.eu/download/5G-XHaul_D_31.pdf.

8 Acronyms

Acronym	Description
3GPP	Third Generation Partnership Project
5G	Fifth Generation Networks
5G-PPP	5G Infrastructure Public Private Partnership
ADC	Analogue-to-Digital Converter
AFE	Analogue Front-End
AWG	Arbitrary Waveform Generator
BITS	Building Integrated Timing Supply
BB	Baseband
BCL	Boundary Clock
BBU	Baseband Unit
BC	Boundary Clock
BH	Backhaul
BMS	Broadcast Microwave Services
BS	Base Station
BWT	Blu Wireless Technology
CFO	Carrier Frequency Offset
COTS	Commercial Off-The-Shelf
C-RAN	Cloud Radio Access Network (aka Cloud-RAN)
D2D	Device-to-Device
DAC	Digital-to-Analogue Converter
DC	Data Centre
DDC	Digital Down-Converter
DFL	Device-Free Localisation
DoA	Direction of Arrival
DP-NLoS	Direct Path NLoS
DUC	digital up-converter
e2e	end-to-end
ESMC	Ethernet Synchronisation Messaging Channel
ETSI	European Telecommunications Standards Institute
FH	Fronthaul
FSM	Finite State Machine
GLONASS	Global Navigation Satellite System
GNSS	Global Navigation Satellite System
GPS	Global Positioning Satellite

I2CAT-UPC	I2CAT Foundation - Polytechnic University of Catalonia
I/Q	in-phase and quadrature
IHP	Innovations for High Performance Microelectronics (Partner-Coordinator)
IoT	Internet of Things
ITU	International Telecommunication Union
KPI	Key Performance Indicator
LAN	Local Area Network
LoS	Line-of-Sight
LTE	Long Term Evolution
MAC	Medium Access Control
MBB	Mobile Broadband
MBMS	Multimedia Broadcast Multicast Services
MCS	Modulation and Coding Scheme
MIMO	Multiple-Input Multiple-Output
MLS	Maximum Length Sequence
mmWave	Millimetre-Wave
NDP-NLoS	Non-Direct Path NLoS
NGMN	Next Generation Mobile Networks
NLoS	Non-Line-of-Sight
NPU	Network Processing Unit
OS	Operating System
OTDoA	Observed Time Difference of Arrival
OTN	Optical Transport Network
p2p	Point-to-Point
p2mp	Point-to-Multipoint
PBSS	Personal Basic Service Set
PLL	Phased-Locked Loop
PON	Passive Optical Network
PRC	Primary Reference Clock
PTP	Precision Time Protocol
QoE	Quality of Experience
RAN	Radio Access Network
RAT	Radio Access Technology
RF	Radio Frequency
RMSE	Root-Mean-Square-Error
RTT	Round-Trip-Time
RU	Remote Unit

SDH	Synchronous Digital Hierarchy
SDR	Software Defined Radio
SONET	Synchronous Optical Network
SotA	State-of-the-Art
STS	Short Training Symbols
SyncE	Synchronous Ethernet
TCL	Transparent Clock
TDD	Time Division Duplex
TDMA	Time Division Multiple Access
UC	Use Case
UE	User Equipment
UL	Uplink
WDM-PON	Wavelength Division Multiplexing Passive Optical Networks
WP	Work Package